Real-time Fluorescence Image-Guided Oncologic Surgery

Suman B. Mondal[1,2], **Shengkui Gao**[3], **Nan Zhu**[4], **Rongguang Liang**[4], **Viktor Gruev**[3], and **Samuel Achilefu**[1,*]

[1]Department of Radiology, Washington University in St Louis, St Louis, Missouri, USA

[2]Department of Biomedical Engineering, Washington University in St Louis, St Louis, Missouri, USA

[3]Department of Computer Science and Engineering, Washington University in St Louis, St Louis, Missouri, USA

[4]College of Optical Engineering, University of Arizona, Tucson, Arizona, USA

Abstract

Medical imaging plays a critical role in cancer diagnosis and planning. Many of these patients rely on surgical intervention for curative outcomes. This requires a careful identification of the primary and microscopic tumors, and the complete removal of cancer. Although there have been efforts to adapt traditional imaging modalities for intraoperative image guidance, they suffer from several constraints such as large hardware footprint, high operation cost, and disruption of the surgical workflow. Because of the ease of image acquisition, relatively low cost devices and intuitive operation, optical imaging methods have received tremendous interests for use in real-time image-guided surgery. To improve imaging depth under low interference by tissue autofluorescence, many of these applications utilize light in the near-infra red (NIR) wavelengths, which is invisible to human eyes. With the availability of a wide selection of tumor-avid contrast agents, advancements in imaging sensors, electronic and optical designs, surgeons are able to combine different attributes of NIR optical imaging techniques to improve treatment outcomes. The emergence of diverse commercial and experimental image guidance systems, which are in various stages of clinical translation, attests to the potential high impact of intraoperative optical imaging methods to improve speed of oncologic surgery with high accuracy and minimal margin positivity.

Keywords

Cancer; surgery; fluorescence; optical; intraoperative imaging; image-guided surgery

1. Introduction

Imaging plays a central role in advancing biomedical and clinical research by providing critical information about molecular and functional processes of normal and diseased states of the body. Today, medical imaging methods have become indispensable in oncologic diagnosis, treatment planning, and monitoring treatment response. In oncology, the need for

---

[*]Corresponding author: achilefu@mir.wustl.edu.

accurate visualization of tumors during surgery to ensure successful removal of all of the cancerous tissue in the first attempt while preserving healthy tissue has spurred the application of image guidance in the operating room. To be successful, the imaging methods are expected to detect tumors in the surgical suite in real-time with high sensitivity and specificity. Importantly, displaying the information in an accessible, easy to comprehend fashion to the surgeon will facilitate adoption of the method in clinics.

Although real-time image guidance is highly desirable in the operating room, it imposes technological hurdles, notably a minimum of 24 frames per second data acquisition and image display. As a result, the imaging time must be short (in the millisecond range) and any image processing must be very fast to allow display of images without latency to the surgeon. An approach to improve tumor-to-background ratio, which is needed for rapid assessment of suspicious lesions, is to incorporate molecular imaging agents in the imaging procedure. Molecular probes suitable for this application have been an area of enhanced research in the last two decades. This review discusses the need for real-time image guidance in oncologic surgery, current methods available for image guidance, along with their limitations and their advantages. Because fluorescence methods hold the most promise for clinical translation, emphasis on fluorescent molecular probes, imaging system design considerations, and current fluorescent image guidance systems highlights the promise and challenges of translating optical methods to humans within the context of oncologic image-guided resection of cancer.

1.1 Need for real time image-guided surgery

Cancer remains a major public health problem in the US and poses a huge economic burden (Yabroff et al., 2011). One in 4 deaths in the USA is caused by cancer (Siegel et al., 2014). Although chemotherapy radiotherapy continue to play major roles in cancer treatment, surgery remains the primary curative option for most solid cancers (Ries et al., 2008). An important goal of oncologic surgery is to remove all cancerous tissue while preserving as much of the healthy tissue as possible. In this process, it is critical to avoid iatrogenic damage to vital organs and anatomic structures. With this overarching goal, delineation of tumors and their infiltration into healthy surrounding tissue will facilitate surgical resection with low margin positivity. Although the primary tumor mass are readily detectable, the boundary of the tumor and microscopic tumors are difficult to identify with unaided eyes.

Currently, preoperative imaging modalities such as magnetic resonance imaging (MRI), computed tomography (CT), and positron emission tomography (PET) provide exquisite structural or functional images that highlight the location of cancerous tissues. These modalities have facilitated early tumor detection, improved diagnostic accuracy, and helped in better staging and preoperative planning (Weissleder and Pittet, 2008). Unfortunately, these systems are not currently amenable to use in the operating room because of their large hardware footprint, slow image reconstruction, lack of microscopic imaging capability, use of ionizing radiation, prohibitive cost, and specialized operator requirement (Jolesz, 2014; Vahrmeijer et al., 2013). Currently, surgeons rely only on their sight and touch to distinguish tumors from surrounding tissue. Human eyes cannot see deeper than the tissue surface, while human touch may not be able to distinguish small tumor nodes from the surrounding

healthy tissue. It is even more difficult to distinguish diffuse tumors from healthy tissue merely by visual inspection and palpation. This may lead to incomplete tumor removal or resection of healthy tissue. Inaccurate delineation of the extent of the tumor tissue can endanger vital structures such as the nerves, leading to iatrogenic damage. Without image guidance, the accurate identification of tumors can be subjective and relies heavily on the surgeon's experience. This creates significant variability in surgical outcomes.

Ex vivo histologic validation of excised tissue is used to determine if the resected tissue harbors tumors on the margins (Fig. 1). In some organs, a significant volume of healthy tissue is removed to minimize the chances of positive margins. However, this luxury is not available for certain organs such as the brain, where debulking of tumors is tailored to avoid disruption of brain functions. In breast cancer patients undergoing breast conserving surgery (BCS), between 20–70% have positive margins, typically indicating the presence of cancerous cells at or near the surgical margins (Collins et al., 2009; Jacobs, 2008; Vicini et al., 2000). Invasive ductal carcinoma (IDC), the most common form of invasive breast cancer, has worse outcome for BCS, due to its poorly-defined tumor boundaries, rendering mastectomy a more reliable procedure (Skripenova and Layfield, 2010). The issue of positive margins is prevalent in cancers at other locations as well. For example the standard 0.5 cm margin recommended for melanoma in-situ leads to 14%–50% of patients with positive margins that need subsequent re-excision (Agarwal-Antal, Bowen and Gerwels, 2002; Kunishige, Brodland and Zitelli, 2012; Moller et al., 2009). Therefore the gold standard remains histopathology, a procedure that renders its verdict after the patient has left the operating room (Jolesz, 2014). These cases generally necessitate repeat surgery, which is not only expensive, but has limited success because of the difficulty in seeing microscopic tumors or diffuse cells. Additionally, scar tissue formation also perturbs the surgical planes, making it more difficult for the surgeon to identify the remnant tumor tissue. Some studies suggested that surgery is a major perturbing factor for metastasis development in lab animals and in breast cancer (Demicheli, Valagussa and Bonadonna, 2001) and that the neovasculature spawned after surgery may actually promote metastatic tumor growth (Retsky et al., 2004). These studies underline the added importance of complete tumor removal in the first surgery. Thus, adoption of real-time image-guided surgery may help in reducing recall rates for oncologic surgery and prevent residual tumors from proliferating because of the perturbations from surgery.

These studies illustrate the tremendous interest in developing intraoperative image guidance systems that can help surgeons to visualize tumors in real-time and improve the accuracy of tumor resection without disrupting the normal surgical workflow. Some general requirements for such a system are summarized in Table 1.

1.2 Current methods available for image-guided surgery

Some traditional imaging methods are currently used for surgical navigation. These include fluoroscopy and intraoperative ultrasonography (IUS). However, X-ray-based techniques such as fluoroscopy suffer from many challenges, including the exposure of patients to ionizing radiation, need for high concentration of contrast agents to compensate for the poor detection sensitivity, inability to detect microscopic lesions, and difficulty in miniaturizing

X-Ray equipment. IUS can be used for tumor detection based primarily on tissue morphology, leading to significant false positive and negative rates (Arii et al., 2010; Kane, 2004; Ukimura et al., 2008; van Vledder et al., 2010). Moreover, IUS is a contact based method, which is less useful for identifying tumor boundaries or microscopic tumors during open surgeries, hampering detection of superficial and small tumors (Sahani et al., 2004). Advanced instruments that mimic global positioning systems have been developed, where preoperative CT or MR image can be projected onto the appropriate anatomical structures. These systems suffer from limitations of the pre-operative imaging method, unsatisfactory registration due to tissue deformation and motion, and the inability to interrogate surgical margins for the presence of tumors. Intraoperative versions of MRI and CT systems have been developed, which are useful for preoperative staging and intraoperative guidance during tumor resection, especially in neurosurgery (Jolesz, 2014). Recent studies have shown that intraoperative MRI has is more effective than conventional neuro-navigation-guided surgery in increasing the extent of glioblastoma multiforme resection, enhancing quality of life, and prolonging survival after surgery (Kubben et al., 2011). However, these systems have a large hardware footprint, require a complex infrastructure, specialized surgical suites and currently configured for neurosurgical applications only (Mislow, Golby and Black, 2009). Using MRI or CT in the operating room severely restricts the reach of the surgeon due to the small area in the scanner bore and the required compatibility of surgical instruments with the system's magnetic field. Additionally, the preoperative view provided by these imaging modalities does not correspond to the field of view of the surgeon, which could disrupt normal surgical workflow. These limitations created a niche for intraoperative optical imaging systems for use in the operating room.

1.3 Optical methods amenable to image-guided surgery

Optical imaging techniques extract diagnostic information from light-tissue interactions. This imaging platform enjoys a combination of interesting features that uniquely makes it amenable to surgical applications. These include the ease of detection, high spatial and temporal resolution, and availability of a wide variety of contrast agents with unique signaling mechanisms. For these reasons, various optical techniques have been developed, which are at different stages of development or clinical translation.

Spectroscopic imaging, for example, uses spectral analysis methods to identify unique optical signatures that are characteristic of a target tissue. This approach has been used extensively to improve early detection of gastrointestinal malignancies (Liu et al., 2007), for intraoperative assessment of breast cancer margins (Wilke et al., 2009) and detection of other forms of cancer (Ramanujam, 2000). The vibrational spectra of biological specimens has been used to identify the biochemical constituents of tissue, but the relatively low sensitivity and limited spatial and temporal resolutions of this technique limits its application for *in vivo* use. Much stronger vibrational signals can be obtained with coherent anti-Stokes Raman scattering (CARS), a nonlinear Raman technique (Evans et al., 2005). CARS microscopy is useful for mapping lipid compartments, protein clusters and water distribution. Utilization of these spectral imaging methods for real-time image-guided surgery has not fully materialized, but they can readily play a role in characterizing focal suspicious lesions in situ. This could accelerate medical decision in the operating room.

Optical coherence tomography (OCT) is another optical technique that is used to provide surgical guidance. OCT is a nondestructive, high-resolution optical approach that uses low-coherence light and interferometry techniques to generate cross-sectional depth resolved two-dimensional (2D) and three dimensional (3D) images (Brezinski, 2006). The technique is similar in principle to ultrasound imaging, but, rather than measuring back reflected sound echoes from the tissue, it measures the amount of backscattered light (Huang et al., 1991). Intraoperative OCT can provide both qualitative and quantitative three-dimensional information. A recent study utilized OCT in many surgical specialties, especially in ophthalmology imaging (Joos and Shen, 2013; LaRocca et al., 2013; Lu et al., 2014; Lucia Pelosini, 2013; Paul Hahn, 2011; Ramiro S. Maldonado, 2010; Tao et al., 2010; Woonggyu Jung, 2012) and coronary imaging (Bouma and Tearney, 1999; Ferrante, 2013; Jang et al., 2002). Intraoperative evaluation of breast tumor margins using OCT has also been reported (Nguyen, 2009). Several commercially OCT systems are available, including portable handheld OCT scanners for intraoperative applications (LaRocca, et al., 2013; Lu, et al., 2014; Palanker et al., 2010; Ramiro S. Maldonado, 2010; Woonggyu Jung, 2012). The handheld OCT scanner can be positioned in close proximity to a patient. The scanning head can be operated from any angle, facilitating the scanning of patients in the supine position. Difficulties with handheld OCT scanners principally involve stability and sterility, which necessitates the wrapping of the OCT probe and attached cord in sterile drapes before use in the operative field. Resolution and reproducibility are limited by operator stability. Newer OCT systems hold more promise for intraoperative applications. Examples include the Bioptigen OCT instrument (Bioptigen, Inc., Research Triangle Park, NC), iVue (Optovue, Inc., Fremont, CA) and Spectralis (Heidelberg Engineering). Wide applications of OCT in the operating room are envisaged in future.

Photoacoustic imaging is an emerging hybrid imaging technology that uses short laser pulses to irradiate chromophores in tissue, inducing localized thermo-elastic expansion that is detectable by wide-band ultrasonic transducers. Photoacoustic tomography offers improved depth resolution in the 3–20 mm range (Poh et al., 2006). Taking advantage of the high absorption coefficient of blood, photoacoustic imaging can display exquisite images of vascular network around tumors without the need for exogenous contrast agents. Ironically, fluorescent dyes with high absorption coefficient but low fluorescent quantum efficiency (which are not optimal for fluorescence imaging) are excellent contrast agents for photoacoustic imaging. A handheld photoacoustic probe system was recently developed for image-guided needle biopsy of sentinel lymph nodes for use in the operating room (Kim et al., 2010). With current efforts to miniaturize the technology, it is hoped that this imaging method could become an enabling platform for diverse surgical procedures.

2. Fluorescence imaging systems for intraoperative procedures

Fluorescence guided surgical resection of tumors—Although methods such as light scattering, absorption spectroscopy, Raman spectroscopy, bioluminescence imaging, and optical coherence tomography continue to make major advances, fluorescence techniques have dominated the field of intraoperative image-guided surgery recently.

Accordingly, the remaining sections of this review focus on current and future status of fluorescence-based methods for real-time image guidance in the operating room.

3.2 Fluorescence sensor parameters

In this section, we consider the detection sensitivity of an imaging system for fluorescent signals. There are many factors that influence the performance of the fluorescence detection. These include the sensors' quantum efficiency in the emission wavelengths of the fluorescent dye, signal-to-noise ratio of the imaging sensor, transmission and optical density of both excitation and emission filters, and optical and electrical crosstalk between photodiodes, which is typically modeled via an overall modulation transfer function of the entire system. All of these effects contribute to the contrast ratio and the signal-to-noise ratio of the fluorescence signal. Each one of these factors is examined in details below.

Quantum efficiency of a photodiode—Quantum efficiency (QE) of a photodiode describes the amount of electron-hole pairs that are generated for a given number of incident photons per wavelength. QE is mathematically modeled via equation (1).

$$QE\left(\lambda\right) = \frac{N_{sig}\left(\lambda\right)}{N_{ph}\left(\lambda\right)} \quad (1)$$

In equation (1), N_{sig} is the signal charge in one pixel, and N_{ph} is the number of incident photon in one pixel. For example, if there are 100 incident photons at 780 nm and 30 electron-hole pairs are generated by the photo detectors, the quantum efficiency of the photo-detector is 30%. Higher quantum efficiency is preferred over lower one in order to detect the smallest amount of emitted photons by the detector. Most imaging sensors are tailored for maximum quantum efficiency in the green wavelengths (~550 nm), where the human visual system is highly sensitive. The quantum efficiency in the NIR is determined by the depth of the p-n (positively doped silicon and negative doped silicon) photo sensitive junction, as well as the doping concentration of the p-n junctions. In silicon photo-detectors, 99% of the incident NIR photons will penetrate and will get absorbed up to 20 microns. Most imaging sensors are fabricated on anepitaxial silicon, where the maximum depth of the photodiode is around 3 to 5 microns. Hence, most of the NIR photons will not get absorbed by the photodiode. This is the chief reason for the poor NIR sensitivity in complementary metal–oxide–semiconductor (CMOS) photo-detectors. Older CMOS process, such as 0.5 micron feature technology, tends to have deeper p-n junction, but they suffer from lower silicon doping. Hence, the overall benefit of deeper junctions is lost and the quantum efficiency in the NIR region remains around 30%. Nevertheless, semiconductor systems can drastically increase quantum efficiency in the NIR, but the size of the market prevents manufacturers from investing in the necessary resources to develop these sensors.

Signal-to-noise ratio (SNR)of an imaging sensor—The SNR is a metric that quantifies the smallest signal that can be detected by the imaging system in the presence of noise. The SNR of an imaging sensor can be computed by the equation (2):

$$SNR = 20log\frac{S}{N}\,[dB] \quad (2)$$

In equation (2), S is the number of electron-hole pairs generated for a given incident photon flux and N is noise in the detected signal.

To understand the SNR performance of a sensor, all noise sources in a sensor should be analyzed. There are two dominant noise sources in an imager. The first noise contributor is the read-out noise of the sensor or the thermal and 1/f noise of the read-out electronics in a sensor. This comprises source follower amplifier and switch transistors in the pixel, current source biasing transistor at the periphery of the imaging array, sample and hold circuit necessary for correlated double sampling operation, and an analog-to-digital converter (ADC). Once the photo-voltage, which is in an analog format, is digitized or quantized, there are no additional thermal noise contributors to the photo-signal. The thermal noise of the reset transistor, also known as reset noise, can be cancelled via a technique known as correlated double sampling (CDS). This technique subtracts the photodiode voltage from a known reference voltage using special charge transfer transistors, a technique borrowed from the charge-coupled device (CCD) imaging arena, and cancelling the thermal noise of the reset transistor. The CDS operation also effectively cancels 1/f noise because subtraction of the two voltages mentioned above is performed at high speed (~10 MHz to ~100 MHz), while the 1/f noise fluctuations have maximum bandwidth of 100 kHz. The biasing circuitry (typically a current mirror or cascoded current mirror), the sample and hold circuitry and the ADC circuitry introduce minimal thermal noise to the photo-signal. Since these circuits are placed outside the imaging array, where silicon real-estate is relatively cheap compared to the pixel's real-estate, which has prime value due to the small pixel pitch requirements, circuit designers utilize the silicon space to design low noise read-out circuits. Today's state-of-the-art imaging sensors have read-out noise close to few electrons, a remarkable feat allowing for extraordinary image quality in low light settings.

The second noise contributor in the imaging system is the photodiode shot noise. The shot noise arises from the uncertainty that an electron-hole pair, which is generated by the absorption of a photon, will pass though the depletion region of the p-n junction. This uncertainty is modeled as a Poisson distribution, which gives the typical approximation estimate of the shot noise power as $N\,e^{-2}$, where N is the total number of generated electron-hole pairs. From the two dominant noise sources, i.e. read-out noise of the electronic circuitry and photodiode's shot noise, the SNR of the imaging sensor can be computed via the equation (3):

$$SNR = 20log\left(\frac{S-B}{\sqrt{n_{read}^2 + n_{photon\,shot}^2}}\right)[dB] \quad (3)$$

It is important to differentiate which one of the two noise sources is dominant and how to optimize the SNR performance for a given illumination conditions (or a photon flux). For low light conditions, the read-out noise is the dominant noise source in the system (Fig. 2).

In this region of operation, the SNR of the imaging sensor can be approximated by equation (4):

$$SNR \approx 20log\left(\frac{S-B}{n_{read}}\right)[dB] \quad (4)$$

Under bright light conditions, the performance of the imaging sensor is limited by the shot noise of the photodiode (Fig. 2). For example, if the read-out noise is 10 e$^-$, and there are 10,000 electron-hole pairs generated by the photodiode, the shot noise will be 100 e$^-$. Since the read-out noise and shot noise powers are added, the total noise in the system is $\sqrt{(10^2+100^2)}=100.5\ e^-$. Hence, the contribution of the read-out noise is 0.5% from the total noise figure in the system and therefore is negligible. The SNR performance of the imaging sensor in this region of operation can be approximated via equation (5):

$$SNR=20log\left(\frac{S-B}{n_{photon-shot}}\right)=20log\left(\frac{S-B}{\sqrt{S}}\right)\xrightarrow{B \ll S} \approx 20log\left(\sqrt{S}\right)[dB] \quad (5)$$

To maximize the SNR performance, the imaging sensor should be used close to the saturation level of the sensor or close to the full well-depth capacity of the pixel. For a given light intensity, the integration time (also known as exposure time) of the sensor can be adjusted such that the total number of integrated electrons does not exceed the total pixel well-depth capacity. Also the integration time should not exceed 33 msec to ensure 33 frames per second read out speed. This will guarantee that the sensor is limited by the shot noise and will give the maximum SNR performance of the sensor. In this configuration, the sensor will be able to discern signal from noise with the highest confidence.

Electrical and optical crosstalk—Electrical and optical crosstalk is another important aspect of the imager performance. The electrical cross talk refers to portion of the electron-hole pairs that are generated by incident photons from one photodiode but registered by neighboring pixels. In other words, the photo-voltage from a given photodiode contains contributions from photons absorbed by this photodiode as well as a portion from photons absorbed from neighboring photodiodes. Today's state-of-the-art imaging sensors try to mitigate this effect via various vertical trenches between photodiodes, but the crosstalk is not completely eradicated. The optical crosstalk is due to the lenses, filters, antireflective coatings and other optical elements used in the imaging system. The effect causes light to reflect and refract multiple times within the imaging system, such that light that should be absorbed by one photo-detector will be absorbed by neighboring photo-detectors.

The electrical and optical crosstalk has two fold negative effects on the performance of the imaging sensor. First, the photodiode signal is diminished because part of the dynamic range is "wasted" on the neighboring photons. Computational models can mitigate this effect at the expense of reduced SNR. The second effect is related to the decrease of resolution or decrease in the modulation transfer function (MTF) of the system. MTF is a measure of the electrical response of the imaging system when a sinusoidal pattern with varying spatial frequency is presented. The amplitude ratio of the sinusoidal function for a given spatial frequency defines the MTF parameter for that particular spatial frequency. Ideally this

number should be 1, but due to low pass filtering from the lenses and optics integrated with the sensor, the MTF tends to decrease with increase of the spatial frequency.

The MTF of the entire imaging system is composed of the MTF of the imaging lens, MTF of the optical filters and MTF of the sensor (Fig. 3). The MTF of the lens is determined by the various lenses included in the lens system, as well as the material used to construct the lenses. The MTF of the optical filter is typically a weak function of spatial frequency and the MTF of the sensor is determined by the pixel pitch and the electrical crosstalk between pixels. The overall MTF function is a product of all three MTF functions as shown by equation (6):

$$MTF_{System}\left(\lambda\right) = MTF_{Lens}\left(\lambda\right) \cdot MTF_{Filter}\left(\lambda\right) \cdot MTF_{Imager}\left(\lambda\right) \quad (6)$$

The mixing of information between a neighborhood of pixels has the same effect as a low pass filtering of the image, which tends to blur the image. Once the image is low pass filtered, high resolution components are removed and details of the image are compromised. These blurring effects are a function of wavelengths due to the dependency of the photon absorption depth as a function of wavelength. Hence, red photons tend to blur images more than blue photons.

Transmission and optical density of excitation and emission filters—
Transmission and optical density of the filters used for both the excitation light source and the emitted light are equality important in the overall imaging sensor design. The transmission wavelength of the excitation light source is tailored to coincide with the maximum absorption coefficient of the dye used to tag the desired molecules. For example, the maximum absorption coefficient of ICG is at about 780 nm. Hence, the emission filter for the light source should allow transmission of 780 nm with high efficiency and block higher wavelengths with high optical density factor. A typical filter in this case will have transmission efficiency of ~90% at 780 nm and optical density of 6 at 800 nm. The emission filter is then placed on the imager side to block the emission light and pass higher wavelengths.

Overall SNR and contrast ratio of fluorescence signal—In most of the fluorescence imaging experiments, background signal could generate large amounts of photons at the same wavelength as the fluorescent light. Therefore, the background interference has to be considered in the SNR computation, and SNR computation using equation (7):

$$SNR = 20log\left(\frac{S-B}{N}\right)[dB] \quad (7)$$

The contrast ratio is the ratio of the fluorescent light intensity to the total incoming light intensity received by the imaging sensor, as shown in equation (8):

$$Contrast\ Ration = \frac{I_{Fluorescent\ Light}}{I_{Total\ Light}} = \frac{I_{Total\ Light} - I_{Leakage\ Light}}{I_{Total\ Light}} \quad (8)$$

The ideal contrast ratio should be 1. However, most organic NIR fluorescent dyes have a narrow band gap between the excitation light and emitting light (narrow Stokes shift), with significant spectral overlap between excitation and emission spectra (Fig. 4). This feature results in significant excitation light leakage, which is reflected by the object in the same emergent angle as the fluorescent light. Therefore, the contribution of the interfering light should be subtracted from the captured light to enhance the detection sensitivity and accuracy. To obtain high contrast ratio and precision, high optical density filters are placed on both imager side and the light source side. The longpass filter on the sensor side eliminates the visible spectrum interference. The bandpass filter on the light source side is used to ensure only the light of appropriate wavelength excites the target tissue.

2.2 Optical design parameters

The design parameters for a fluorescence imaging system include the power and homogeneity of the excitation light, the field of view (FOV) and numerical aperture (NA) of the detection system that collects the emission light, the sensitivity and noise characteristics of the detector, and the transmission and blocking capabilities of the fluorescence filters.

At low concentration of molecular probes in tissue, fluorescence signals are usually weak and require long exposure time for data acquisition. Therefore, the design of an optical system for fluorescence analysis must consider the entire optical path. Low fluorescence signal requires a highly efficient optical system to improve light-capturing abilities for a higher throughput, to provide a higher dynamic range that accommodates the vast differences in fluorophore concentrations across the sample, and to reduce crosstalk between sample spots through improved optical resolution.

Lens and filter strategy—The basic requirements for good fluorescence detection systems include high-resolution and high-fluorescence signal collection and transmission. Generally, high resolution and high light-collection efficiency are related through the NA. The larger the NA is, the higher the resolution and light-collection efficiency. In cases where the fluorescence signal is more critical than the resolution, the imaging lens is often designed with a large NA, but a lower aberration correction (fewer optical elements). As a general guideline, the optical elements in the detection and excitation paths should be as few as possible to increase light transmission and minimize the autofluorescence of the optical components.

An infinite-conjugate imaging system is preferred, but not required, when the excitation and emission share the same objective lens, so that the dichroic mirror and other components can be inserted or removed between the objective lens and the tube lens without introducing aberrations and image shift. Generally, a telecentric imaging system is desirable, especially for off-axis point scanning, so that the collection efficiency of fluorescence signal is uniform across the entire FOV.

The transmission of both the excitation and emission light should be as high as possible. Antireflection (AR) coatings are essential for achieving high transmission. Depending on the excitation and emission wavelengths, as well as the locations of the optical elements, various types of coatings can be applied. For optical elements used in both the excitation and

emission paths, either a W-shaped AR coating with two minimal reflection bands or a broadband AR coating is required. For elements used only in the excitation path, a V-shaped AR coating is enough to minimize the reflection of the excitation light. Similarly, a V-shaped AR coating with minimal reflection at the emission wavelength can be sufficient for the elements in the detection path.

Most of optical glasses and plastics have good transmission performance in NIR spectrum up to 1500 nm or even longer. Therefore, a traditional lens designed for visible spectrum can be used in the spectrum for fluorescence image-guided surgery. The optical surfaces in a visible lens are normally optimized for visible spectrum (400–700 nm). For use in fluorescence image-guided surgery, optics with surface coating optimized for NIR is needed to have maximum transmission in the working spectrum.

To optimize the detection of a fluorescence signal, excitation filters are selected to maximize blocking in the transmission passband of the emission filter in the illumination path and to maximize blocking in the corresponding transmission passband of the excitation filter in the detection path. In general, it is preferable to block out-of-band light with an excitation filter instead of an emission filter so that the sample will be exposed to less radiation. In addition, fewer components and less-complicated optical systems re required in the detection path.

The optimal position of the excitation filter is where the range of the ray angle is small and away from the light source to reduce the angular effect of the optical coatings and autofluorescence of the components in the illumination path. The emission filter should be placed in front of other optical components in the detection path to reduce autofluorescence from those components. However, in many applications, it is not practical to place the emission filter as the first element. For a very compact device where there is not enough space for the emission filter in front of the objective lens, the next optical location is where the range of the ray angle is small.

Illumination design—In fluorescence imaging, it is desirable to closely match the excitation wavelength of the light source with the maximum excitation wavelength of the fluorophore to achieve a high-contrast image. Wavelength is also the major factor in determining the imaging depth because the penetration depth of light in tissue strongly depends on the wavelength. Light-source intensity is another factor in fluorescence imaging; it determines how much excitation light can reach the sample. For fluorophores with low quantum yields, high power light sources are needed to sufficiently excite enough molecules for fluorescence capture by detectors such as a photomultiplier tube (PMT), avalanche photodiodes (APDs), a CCD, or a CMOS sensor. The human eye is less sensitive than most electronic detection systems, and thus, applications involving visual observation require higher levels of illumination intensity.

Noncoherent and coherent light sources are used in fluorescence imaging. Noncoherent light sources are usually broadband and are typically used in fluorescence spectrometers and large area imaging systems. The spectral output of noncoherent light sources can be tuned to a narrow band of excitation light or a predefined spectrum by using gratings, filters, and spatial light modulators, such as liquid crystal devices or digital micromirror devices.

Mercury and xenon arc lamps are the most common noncoherent light sources used in fluorescence imaging. Historically, mercury high-pressure arc lamps (commonly referred to as HBO lamps) were the most prevalent light source for fluorescence imaging. The light intensity of a mercury lamp is not evenly distributed from ultraviolet (UV) to NIR region, with peaks of intensity at 313, 334, 365, 406, 435, 546, and 578 nm. Between these peaks, the excitation energy of the light source is very low. If these lines coincide with or are close to the peak of the fluorophore's excitation spectrum, a mercury lamp is the optimal light source. HBO lamps are suitable for applications that need blue or UV light to excite fluorescence. They typically have a short life span (~300 hours), necessitating relatively frequent bulb changes.

In contrast, xenon arc (XBO) lamps have a relatively flat emission across the visible spectrum. The uniform emission levels and lower fluctuations make XBO lamps better suited for applications in ratio imaging and other quantitative applications. XBO lamps also have stable emission intensity over time, contributing to the long life span of these lamps (400–2000 hours).

The xenon-mercury arc lamp has the best characteristics of both xenon and high-pressure mercury lamps. The spectral distribution of a mercury-xenon lamp includes a continuous spectrum from the UV to the infrared and the strong mercury line spectrum. This combination is an ideal source for some applications because it provides extremely high excitation energy over large spectral bandwidth.

Metal halide (HXP) white-light sources have an emission spectrum similar to that of mercury lamps. HXP lamps have an emission output featuring pressure-broadened versions of the prominent mercury arc spectral lines in addition to higher radiation levels in the continuous regions between lines. Therefore, HXP lamps usually produce much brighter images of fluorophores, which have absorption bands in the spectral regions between the mercury lines. Commercial HXP lamps have extended arc-lamp lifespans (up to 2000 hours).

To eliminate traditional alignment problems and provide uniform illumination across the entire FOV, a liquid light guide or fiber light guide is often used to couple the light out from the arc lamp. The light guide acts as a scrambler to homogenize the arc output and create an even field of illumination. The light guide also has the advantage of reducing heat transfer from the light source to the sample.

One advantage of arc lamps is that one light source can be used to excite several fluorophores independently or to excite several fluorophores simultaneously. They can also be used as a light source for white-light illumination. One disadvantage of using arc lamps is that one or more filters are required to select the spectrum for optimal fluorescence excitation. There are several other issues related to arc lamps. The bulbs may explode because of high working temperatures and pressures, although the possibility of explosion is low. For all gas-discharge lamps, reaching optimal working conditions usually takes time, and restarting them after they are turned off requires a certain period of time. The light intensity may fluctuate and drop throughout the lifetime of the lamp.

For simple fluorescence imaging systems, the excitation light is delivered directly to the sample from a light source without any additional optics. For most fluorescence imaging systems, illumination optics is needed for efficient and uniform delivery of the excitation light to the sample. Because of the relatively weak fluorescence signal, the efficiency of the light delivery system becomes critical to optimize fluorescence imaging systems. Thus, uniform illumination is required because the fluorescence signal at each point is proportional to the illumination light at that location. Beam-shaping elements (such as a lenslet array, light pipe, or aspheric elements) are usually used to provide spatially uniform excitation light to the samples. For some applications, an array of light sources, typically LEDs, provide sufficient excitation light with reasonable uniformity.

It is also important to protect the sample, especially in live-cell imaging applications, from overexposure and heat from the light source during illumination. This can be achieved by attenuating the light intensity and by limiting the duration of the illumination to exactly the exposure time of the sensor.

3. Current Intraoperative Optical Image guidance Systems

Several complete intraoperative NIR fluorescence imaging systems are now available for pre-clinical and clinical studies (Gioux, Choi and Frangioni, 2010; Schaafsma et al., 2011b). Although differing in their technical specifications, all of these systems provide the surgeon with an image of the NIR fluorescence signal that would otherwise be invisible to the human eye (Table 2). Some of these systems have been approved by the U.S. Food and Drug Administration (FDA) for use in humans. For example, the Novadaq SPY system is an intraoperative imaging system that uses indocyanine green (ICG) fluorescence for a variety of surgical procedures, including for guidance in coronary artery bypass grafting, plastic and reconstructive surgeries, and organ transplant (Coles et al., 2003; Takahashi et al., 2004). Another system, the photodynamic eye (PDE) developed by Hamamatsu is a handheld imaging system that can detect ICG fluorescence. The majority of clinical studies published to date use this imaging system to identify sentinel lymph nodes (SLNs) in breast cancer patients (Tagaya et al., 2008) and to perform image-guided surgical resection of hepatocellular carcinoma (HCC) (Gotoh et al., 2009). Other commercially available handheld imaging systems are Fluobeam (Fluoptics, France) and Artemis (Quest Medical Imaging BV, Netherlands). They are capable of perfusion imaging, and display the acquired information in a remote monitor.

Because of the clear advantage of these fluorescence image-guided systems for intraoperative procedures, a variety of newer experimental systems have emerged in various laboratories and evaluated in humans. These include the fluorescence assisted resection and exploration (FLARE) system and head mounted display devices.

The FLARE system is an intraoperative real-time imaging system developed by the Frangioni team. This system has been successfully used for SLN mapping in breast cancer patients (Troyan et al., 2009). A smaller and more portable version has also been developed and validated for SLN mapping in human breast cancer patients (Mieog et al., 2011). Other successful applications of this system include the SLN imaging in cervical (van der Vorst et

al., 2011) and vulvar (Hutteman et al., 2012) cancer patients. Although the FLARE system can detect NIR fluorescence with high sensitivity in real-time, it is not portable and has a large hardware footprint.

Another experimental fluorescence image-guided system in early stages of clinical studies is a goggle assisted imaging and navigation system for intraoperative image guidance (Liu et al., 2011). Initial prototypes have been validated in extensive small animal studies (Liu et al., 2013a; Liu et al., 2013b) and also shown to work well in HCC detection in human patients (Liu et al., 2013c). Further improvements were made in the system to improve wearability and video rate image display. The current system is capable of detecting both color and fluorescence signals from the surgical bed using a very small camera. Using fast processing, real-time superimposed images are displayed on the head mounted display worn by a surgeon. This allows image guidance without any disruption of the normal surgical workflow (Fig. 5). High detection sensitivity, ease of usage, ergonomic design and wearablity make it an attractive candidate for wide clinical adoption. At Washington University in St. Louis, the system is undergoing pilot human studies with breast cancer and melanoma patients. Using ICG as the contrast agent for SLN mapping the goggles system compared favorably against traditional radioactive and blue dye methods (unpublished work).

Other experimental systems under development for clinical applications are making significant progress. For example, the HyperEYE system was successfully used for intraoperative graft assessment using ICG fluorescence (Handa et al., 2010). A frequency domain photon migration (FDPM) system was developed for integration into commercial small animal imaging scanners for fluorescence tomography (Darne et al., 2012). It has now been used for non-invasive dynamic lymphatic mapping in humans (Marshall et al., 2010). Finally, a multispectral fluorescence imaging system, SurgOptix, was developed (Themelis et al., 2009) and used to assess SLN detection in cervical (Crane et al., 2011) and ovarian (van Dam et al., 2011) cancer patients.

4. Fluorescent agents used in image-guided surgery

Fluorescence imaging techniques are able to report molecular events with exceptionally high detection sensitivity because of the low background signal prior to excitation of the target tissue with light of the appropriate wavelength. The high detection sensitivity clearly favors the application of fluorescence in image-guided surgery. Fluorescence signal can be mediated by endogenous or exogenous fluorophores. The differential expression of endogenous fluorophores (autofluorescence) or selective accumulation of extrinsic fluorescent molecular probes in the diseased versus normal tissue provides the source of contrast for fluorescence imaging (Table 3).

4.1 Endogenous fluorophores

Tissues and cells express some biomolecules that can serve as a source for autofluorescence imaging. These biomolecules are typically upregulated or downregulated in diseased versus healthy tissues. In autofluorescence imaging, the tissue may be excited by UV, visible, or NIR light with sufficient irradiance to induce specific fluorescence for diagnostic purposes

(Andersson et al., 1998; Croce et al., 1996). In particular, autofluorescence-based spectroscopic imaging has been used for clinical differentiation of cancerous, inflamed and normal tissue in cervical cancer patients (Ramanujam et al., 1994), and for the diagnosis of bladder cancer (Koenig et al., 1996). Simple handheld devices has been shown to identify oral cancer (Poh, et al., 2006) and decrease oral cancer recurrence rate in human patients (Jayaprakash et al., 2009; Poh et al., 2009). To visualize these lesions, intravital and other microscopic techniques are widely used in autofluorescence imaging (Alexander et al., 2008), as demonstrated by their use to distinguish malignancies from benign and healthy tissues (DaCosta, 2003).

A major advantage of autofluorescence imaging and spectroscopy in the context of intraoperative image-guided surgery is that exogenous fluorophore are not needed. With minimal regulatory hurdles compared to the use of exogenous fluorescence dyes or nanomaterials, the approach is readily translatable to clinics. If the goal is to detect microscopic lesions or clearly define tumor boundaries in real time, low tumor-to-background autofluorescence signal may be inadequate. In addition, the shallow penetration of light in the UV and visible spectrum (~400–600 nm) allows the sampling of only superficial tissue. Recent application of intravital multiphoton microscopy promises to improve the imaging depth and spatial resolution, but requires sufficiently large field of view and real-time image display to be practically useful to guide surgical resection of tumors.

4.2 Exogenous fluorescent agents

To overcome some of the above challenges of autofluorescence imaging, exogenous imaging agents are widely used to enhance signal specificity, interrogate molecular events, and improve tumor-to-background contrast in intraoperative fluorescence guided surgery. Exogenous fluoresce is generally provided by synthetic dyes or nanoparticles. The use of exogenous dyes for fluorescence imaging has been in existence as early as 1955, when fluorescent porphyrin was administered and used to detect tumors (Rassmussen-Taxdal, Ward and Figge, 1955). Although many fluorescent agents in clinical use are not designed to target specific tissue, efforts to improve detection specificity and sensitivity have led to the development of tumor-targeted or activatable molecular imaging probes. Earlier studies focused on visible fluorophores because of the availability and experience in handling those dyes, as well as the potential to visualize the emitted light with the unaided eye. However, new emphasis on low background signal and improvement in imaging depth has stimulated interest in the development of NIR fluorophores and dedicated camera systems for image-guided oncologic surgery. Human tissue has low optical absorption and scattering in the NIR window (600 to 1000 nm) that can allow the NIR light to penetrate several centimeters or even further in tissue (Lee et al., 2010; Troyan, et al., 2009). The narrow NIR window between 750 and 900 nm is particularly useful to minimize tissue autofluorescence (Adams et al., 2007; Sevick-Muraca, 2008). Recent studies suggest that the 1300 nm spectral range further improves imaging depth (Lim et al., 2003) and has generated interest in the second optical window of 1000 nm – 1350 nm which can afford much higher depths of penetration (Smith, Mancini and Nie, 2009). An additional benefit of working in the NIR spectrum is that human eyes are insensitive to this light, thereby minimizing interference with the

surgical field, especially under conditions where high intensity continuous or pulsed light source is used (Sexton et al., 2013). The most widely used fluorescent agents for fluorescence image-guided surgery in human patients are summarized below.

Fluorescein—Fluorescein was one of the early dyes used to highlight tumors against surrounding normal tissue (Moore, 1947). The first clinical report of fluorescence imaging in the operating room dates back to 1948, when Moore *et al.* (Moore, Peyton and et al., 1948) used fluorescein to localize brain tumors during neurosurgery. Specific visualization of colorectal carcinomas *in vivo* in patients was accomplished by labeling carcinoembryonic antigen-targeted antibody with fluorescein. This bioconjugate selectively binds to the antigen overexpressed on colon cancer cells. The study was vital in demonstrating the clinical potential of this approach during surgery (Folli et al., 1992). Although antibodies are highly specific for their target antigens, the slow clearance from circulation contributes to high background fluorescence for several days. As a result, small ligands for cell surface receptors overexpressed by tumors are viable alternatives to large biomolecules because their fluorescein derivatives can achieve rapid extravasation, tumor uptake, and excretion of the unbound molecular probe from circulation. An example of this approach is the use of folate-fluorescein conjugate to visualize ovarian cancer intraoperatively and to guide cancer debulking in the operating room (van Dam, et al., 2011). Although these landmark studies successfully demonstrate the feasibility of using fluorescein for fluorescence guided surgery, fluorescein suffers from the limitation of most visible dyes. These include high autofluorescence that could confound image analysis, and shallow penetration of light that only interrogates superficial lesions.

Methylene Blue—Methylene blue is a small molecular weight dye that is widely used in many intraoperative procedures. The ease of visualizing the dark blue color of methylene blue with unaided eyes during surgery facilitated its use for sentinel node mapping. However, high concentration of this dye is needed to visualize the blue color (absorption mode). Recent studies have shown that methylene blue fluorescence at about 700 nm can provide a mechanism to detect the distribution of this dye with highly sensitive sensor systems (Gioux, Choi and Frangioni, 2010; Vahrmeijer, et al., 2013). This high detection sensitivity of the fluorescence signal facilitates the use of low doses of this dye for image-guided surgery, thereby minimizing the side effects of the dye in some patients. This fluorescence approach has found wide application in identifying the ureters during surgery (Matsui et al., 2010), detecting extrahepatic bile ducts, (Matsui, et al., 2010) and assessment of cardiac perfusion (Tanaka et al., 2009). The dye has also been applied to the detection of neuroendocrine tumors, such as insulinoma (Winer et al., 2010a). Although some studies have demonstrated that methylene blue can accumulate in some tumors, this uptake can be sporadic and depends of the tumor type. In addition, relatively high concentration must be used to overcome autofluorescence. Because of the need to detect small tumors during surgery, methylene blue may not be suitable for image-guided surgical margin assessment in real-time. The dye also suffers from limitation of other visible dyes because of the excitation in the 600 nm range.

5-Aminolevulinic acid—5-Aminolevulinic acid (5-ALA) is a small molecule involved in the early phase of porphyrin biosynthesis, which is responsible for heme production in mammals. Through this pathway, 5-ALA serves as the major substrate for protoporphyrin IX (PpIX) synthesis, a naturally fluorescent molecule that is overexpressed in cancerous tissue, especially malignant gliomas and meningiomas. 5-ALA has been used clinically for tumor detection (fluorescence imaging) and treatment (photodynamic therapy). The compound, which is typically administered in topical or oral form, induces the biosynthesis and accumulation of PpIX in epithelial and neoplastic tissues (Colditz, Leyen and Jeffree, 2012; Stummer et al., 2006). PpIX has two major emission peaks, with its second emission peak centered at 700 nm, which is at the fringes NIR fluorescence. A growing area of application is in managing brain cancer. For example, the PpIX precursor has been used for quantitative fluorescence imaging and debulking of gliomas (Brouwer et al., 2012b) and for image-guided resection of glioblastoma, where it was shown to improve tumor free survival in patients (Stummer, et al., 2006). Previous studies reported the use of 5-ALA as a biomarker for distinguishing normal brain tissue from low and high grade gliomas via quantitative fluorescence imaging of PpIX (Valdes et al., 2011). 5-ALA has also been used to identify urothelial cancer using fluorescence guided cystoscopy(Jocham, Stepp and Waidelich, 2008). A persistent concern with 5-ALA approach is the poor sensitivity and a negative predictive value, especially for surgical guidance of glioma resection (Moiyadi, Syed and Srivastava, 2014).

Indocyanine Green—ICG is the workhorse imaging agent for NIR fluorescence image-guided surgery in human subjects because it is currently FDA approved for use in humans (Schaafsma et al., 2011a). ICG can be excited at 780 nm and the fluorescence is captured around 810 – 830 nm (Kraft and Ho, 2014). In blood, ICG interacts with lipids and plasma proteins which enhance its NIR fluorescence and increase its hydrodynamic diameter (Kraft and Ho, 2014). This allows ICG to remain in circulation for a longer duration and accumulate in tumor via the enhanced permeability and retention effect, before being cleared through the liver (Vahrmeijer, et al., 2013). Intravenous ICG injection is currently used for NIR angiography of blood vessels (De Grand and Frangioni, 2003; Matsui et al., 2009; Tanaka, et al., 2009), identification of the extrahepatic bile ducts (Matsui, et al., 2010), and identification of liver metastases (Aoki et al., 2008). Subcutaneous ICG injection has been used for sentinel lymph node (SLN) mapping in breast cancer (Troyan, et al., 2009), gastric cancer (Miyashiro et al., 2008; Nimura et al., 2004), gastrointestinal cancer (Kusano et al., 2008), skin cancer (Fujiwara et al., 2009) and squamous cell carcinoma (Tsujino et al., 2009). The major limitation of this imaging agent is the lack of specificity for tumors. New NIR molecular probes targeted to tumors have shown impressive results in preclinical studies. Unfortunately, these molecular probes have not been approved for use in humans by the US FDA.

5. Clinical Applications of Fluorescence Image-Guided Surgery

Fluorescence-guided surgery is widely used today in oncologic and other intraoperative procedures (Nguyen and Tsien, 2013; Vahrmeijer, et al., 2013). Most of the clinical studies have focused on NIR fluorescence. Because the human eye is not sensitive for light in the NIR region, dedicated camera systems are required to detect the fluorescence signals

emission from these molecules. Fluorescence imaging instruments are relatively inexpensive, simple and can be very compact to adapt many kinds of surgeries. However, optical image guidance has certain limitations and scope. For example, tumors that have a high incidence of positive margins would mostly benefit from this procedure. The choice of contrast agent and its application route is determined by the patient tolerance to the contrast agent and the anatomical position of the area of interest. The major areas of oncologic applications are summarized below.

5.1 Sentinel Lymph Node Mapping

The SLN is the first drainage site of disseminating cancer cells from the primary tumor. Thus, the SLN positivity or negativity is used to stage the metastatic potential of some solid tumors (Tanis et al., 2001). Negative SLN suggests that the tumor is confined to the primary tissue, and could be readily treated by surgical resection. In contrast, positive SLN suggests the potential of cancer metastasis, which triggers a high level of diagnostic assessment and therapeutic regimens. SLN staging is frequently used in the staging of breast cancer and melanoma, and the procedure is under investigation for use in colorectal, gastric, esophageal, head and neck, thyroid, and non-small cell lung cancers (Chen et al., 2006). During SLN biopsy, the tissue is first identified and removed for histologic verification of the lymph node status. Currently, SLN mapping is performed by tracking a radiotracer, a visible blue dye, or a combination of both radiotracer and dye (Giuliano et al., 1994; Morton and Bostick, 1999).

Blue dyes such as methylene blue are injected in the vicinity of the primary tumor and allowed to drain to the sentinel lymph node. Because of the high concentration of the injected dose, the stained tissue is readily visible with the naked eye. Since the human eye can only visualize superficial tissue, this technique is complemented by administering tracer levels of radionuclides. Using a gamma counter, the radioactivity is track to identify the general location of the SLN, which can then be confirmed by visualizing the blue dye. In addition to the poor detection sensitivity of the blue dyes, the procedure exposes health professionals to frequent ionizing radiation and the gamma probe suffers from poor spatial resolution (van den Berg et al., 2012). In contrast, NIR fluorescence imaging with dyes such as ICG enables detection of the SLN with high sensitivity at low doses of a fluorescent dye. ICG passively accumulates in SLNs, but the small size of the molecule facilitates its further migration to adjacent nodes. To address this issue, SLN selective tracer was designed to bind mannose-binding protein receptor found in reticuloendothelial cells of lymph nodes (Vera et al., 2001). This agent has satisfactory performance both as a radiolabeled and fluorescent imaging agents for SLN detection (Ting et al., 2010) It was recently approved by the FDA for SLN mapping based on results from a phase 2 clinical trials in breast cancer and melanoma patients (Leong et al., 2011).

Although the NIR fluorescence imaging approach improves imaging depth, good resolution images are still confined to 5–15 mm deep from the tissue surface. To address this limitation, a combination of NIR fluorescence and radioactive tracers are currently used for SLN mapping in head and neck melanoma (Brouwer et al., 2012a; Brouwer, et al., 2012b), prostate cancer (van der Poel et al., 2011) and squamous cell carcinoma of the oral

cavity(van den Berg, et al., 2012). Future studies will determine potential of using NIR fluorescence imaging without the need for administering radioactive materials (van der Vorst et al., 2012a).

5.2 Tumor Imaging

A major application of real-time fluorescence –guided surgery is to visualize tumors in the operating bed in real-time. ICG was first used clinically to visualize colorectal hepatic metastases and HCC (Ishizawa et al., 2009). Different spatial distribution of ICG in liver tumors has been reported, ranging from a rim of fluorescence around hepatic metastases to localize fluorescence within HCC (Gotoh, et al., 2009; Ishizuka et al., 2012; Peloso et al., 2013; Uchiyama et al., 2010). A recent report suggests that ICG-mediated NIR fluorescence image-guided surgery could identify small HCC nodules in the liver, which was not detected by preoperative CT (Satou et al., 2013). Similar findings were reported in the detection of hepatic metastases of pancreatic cancer (Yokoyama et al., 2012) or colorectal metastases (Vahrmeijer, et al., 2013) in the liver that were not visible by preoperative CT, MR, intraoperative US, visual inspection, or palpation. These studies illustrate the potential of using fluorescence image guidance to survey the operating bed and ensure the removal of small tumor lesions that could readily be missed during surgery. Beyond focused tumors, ICG videography was successfully used for image-guided resection of spinal cord hemangioblastoma (Hwang et al., 2010), CNS tumors(Ferroli et al., 2011) and dynamic imaging during hemangioblastoma surgery (Hojo et al., 2013).

Other than ICG, methylene blue has served as important cancer imaging agent because of its intrinsic affinity to cancer cells. This important feature has been known several decades ago, including the selective staining of parathyroid glands after high dose intravenous injection of the dye (Keaveny, Fitzgerald and McMullin, 1969) or detection of insulinomas after intra-arterial injection (Keaveny, Fitzgerald and McMullin, 1969; Keaveny, Tawes and Belzer, 1971). Recent studies have now demonstrated successfully the use of methylene blue fluorescence to identify insulinomas in preclinical models (Winer, et al., 2010a) and as well as visualizing rare solitary fibrous tumors of the pancreas in a patient (van der Vorst et al., 2012b), though it remains to be clinically approved for insulinoma imaging. The application of 5-ALA in image-guided surgery was discussed above. With the ongoing development of new fluorescent systems for surgical applications, it is important to identify areas of high clinical impact in order to support the introduction of another imaging tool into the already hectic surgical environment.

Protecting vital organs is critical during oncologic imaging because surgery can cause unintended iatrogenic damage to vital structures such as the nerves or sensitive surrounding tissue. For example, nerve damage during rectal cancer surgery may cause urinary and fecal incontinence (Wallner et al., 2008), while nerve damage during bladder and prostate cancer surgery may result in sexual dysfunctions (Miranda-Sousa et al., 2006). Damage to ureters or bile duct may lead to renal dysfunction and biliary peritonitis (Flum et al., 2001; Selzman and Spirnak, 1996). ICG, which is removed from circulation by the liver, is used for intraoperative NIR fluorescence cholangiography (Ishizawa et al., 2010; Spinoglio et al., 2013). The clinical significance of preserving vital organs has stimulated the development of

simple dyes that selectively accumulate in specific tissue, as well as high throughput fluorescence imaging devices for real-time delineation of these tissues during surgery.

6. Future Directions

With recent advances in molecular medicine, high resolution and wide FOV systems could inform clinical research about molecular processes pertinent to the disease in real-time (Weissleder and Pittet, 2008). By coupling imaging with optional therapy, it is anticipated that the procedure will also guide treatment planning and monitor treatment response. These efforts could improve patient outcomes, reduce hospital revisits, and enhance the quality of life. Some specific areas for improvement are summarized below.

From molecular imaging perspective, cancer-targeted fluorescent molecular will improve the specificity and sensitivity of fluorescence-guided surgery. The molecular agents could be designed for instant activation of fluorescence after topical application during surgery to improve the tumor-to-background fluorescence. New activatable molecular probes were recently reported to have this desirable property (Mitsunaga et al., 2013). An alternative approach is to design fluorescent molecular probes that can be trapped in cancer cells for several days, allowing the surgeons flexibility to conduct surgery at any time during that period (Liu, et al., 2011; Liu et al., 2012).

From device development perspective, the rapid development of CMOS process and modern digital imaging technology has improved the performance of recent CMOS imaging sensor used in fluorescence imaging system. High performance sensors can provide more accurate and stronger fluorescence signal as image output. Using the latest 130 nm – 180 nm analog fabrication process, commercial CMOS imaging sensor are optimized to obtain high SNR and much higher image resolution than previous systems. Furthermore, vertically stacked 3-D technology offers high resolution of pixel array, and nearly 100% fill factor by stacking photodiode structure, row/column readout circuit, and storage logic onto different layers. Although the fabrication process of 3-D chip still needs a lot of optimization, it provides an alternative way for CMOS sensor to achieve high resolution and better sensitivity (Zhang, Shoushun and Culurciello, 2011). Finally, imaging sensor research on detection of special light property has increased recently. For example, recent development of division of focal plane polarization imaging sensor enables real-time, high resolution polarization detection, which could be embedded in future fluorescence imaging system for additional polarization information detection (Gruev, Perkins and York, 2010).

System-on-chip (SOC) CMOS imaging sensor can offer flexibility in fluorescence imaging system design. By moving ADC readout circuitry and image pre-processing unit on chip, the imaging sensor system becomes much more compact and power efficient (Johansson et al., 2011). Further reduction in the size and weight of the sensor system is achieved because less peripheral circuits and components are needed for SOC sensor system. This configuration will benefit the compact fluorescence imaging system design.

7. Concluding Remarks

Real-time image-guided surgery is gaining interest because of its potential to improve patient outcome following oncologic surgery. Not only can this approach guide intraoperative surgical margin assessment, the approach is uniquely positioned to detect microscopic tumors or residual lesions that are readily missed during surgery. Numerous types of optical imaging devices are available today to guide surgery. With the ever increasing miniaturization capability, simpler, smaller, and more efficient optical imaging systems will become available for clinical use in high and low resource clinical centers. Current bottleneck preventing full realization of the potential benefits of NIR fluorescence guided surgery is the lack ok FDA approved tumor-selective molecular imaging agents. This missing link is expected to be rectified soon because of dedicated efforts by many investigators and some federal funding agencies such as the National Institutes of Health to support early phase clinical trials with novel imaging agents. Beyond identifying tumors, coupling therapeutic options to either the device or molecular probe arm of the technology could further enhance its potential clinical impact. 5-ALA is currently capable of achieving this goal by providing both imaging and therapeutic capabilities. Alternative theranostic platforms can be developed to harness the modular design of contrast agents and light-triggered drug release.

References

Adams KE, Ke S, Kwon S, Liang F, Fan Z, Lu Y, et al. Comparison of visible and near-infrared wavelength-excitable fluorescent dyes for molecular imaging of cancer. Journal of Biomedical Optics. 2007; 12:024017–024019. [PubMed: 17477732]

Agarwal-Antal N, Bowen GM, Gerwels JW. Histologic evaluation of lentigo maligna with permanent sections: implications regarding current guidelines. Journal of the American Academy of Dermatology. 2002; 47:743–748. [PubMed: 12399768]

Alexander S, Koehl G, Hirschberg M, Geissler E, Friedl P. Dynamic imaging of cancer growth and invasion: a modified skin-fold chamber model. Histochemistry and Cell Biology. 2008; 130:1147–1154. [PubMed: 18987875]

Andersson, Baechi, Hoechl, Richter. Autofluorescence of living cells. Journal of Microscopy. 1998; 191:1–7. [PubMed: 9723186]

Aoki T, Yasuda D, Shimizu Y, Odaira M, Niiya T, Kusano T, et al. Image-guided liver mapping using fluorescence navigation system with indocyanine green for anatomical hepatic resection. World J Surg. 2008; 32:1763–1767. [PubMed: 18543027]

Arii S, Tanaka S, Mitsunori Y, Nakamura N, Kudo A, Noguchi N, et al. Surgical strategies for hepatocellular carcinoma with special reference to anatomical hepatic resection and intraoperative contrast-enhanced ultrasonography. Oncology. 2010; 78(Suppl 1):125–130. [PubMed: 20616594]

Bouma BE, Tearney GJ. Power-efficient nonreciprocal interferometer and linear-scanning fiber-optic catheter for optical coherence tomography. Optics Letters. 1999; 24:531–533. [PubMed: 18071562]

Brezinski, ME. Optical Coherence Tomography: Principles and Applications. Academic Press; 2006.

Brouwer OR, Buckle T, Vermeeren L, Klop WM, Balm AJ, van der Poel HG, et al. Comparing the hybrid fluorescent-radioactive tracer indocyanine green-99mTc-nanocolloid with 99mTc-nanocolloid for sentinel node identification: a validation study using lymphoscintigraphy and SPECT/CT. Journal of Nuclear Medicine. 2012a; 53:1034–1040. [PubMed: 22645297]

Brouwer OR, Klop WM, Buckle T, Vermeeren L, van den Brekel MW, Balm AJ, et al. Feasibility of sentinel node biopsy in head and neck melanoma using a hybrid radioactive and fluorescent tracer. Annals of Surgical Oncology. 2012b; 19:1988–1994. [PubMed: 22207047]

Chen SL, Iddings DM, Scheri RP, Bilchik AJ. Lymphatic mapping and sentinel node analysis: current concepts and applications. CA: A Cancer Journal for Clinicians. 2006; 56:292–309. quiz 316–297. [PubMed: 17005598]

Colditz MJ, Leyen K, Jeffree RL. Aminolevulinic acid (ALA)-protoporphyrin IX fluorescence guided tumour resection. Part 2: theoretical, biochemical and practical aspects. Journal of Clinical Neuroscience. 2012; 19:1611–1616. [PubMed: 23059058]

Coles C, Taggart D, Choudhary B, Abu-Omar Y, Balacumaraswami L, Pigott D. The use of a novel imaging technique to evaluate patency of coronary grafts. Anaesthesia. 2003; 58:304.

Collins L, Schnitt S, Achacoso N, Haque R, Nekhlyudov L, Fletcher S, et al. Outcome of Women with Ductal Carcinoma In Situ (DCIS) Treated with Breast-Conserving Surgery Alone: A Case-Control Study of 225 Patients from the Cancer Research Network. Modern Pathology. 2009; 22:34A–35A.

Crane LM, Themelis G, Pleijhuis RG, Harlaar NJ, Sarantopoulos A, Arts HJ, et al. Intraoperative multispectral fluorescence imaging for the detection of the sentinel lymph node in cervical cancer: a novel concept. Molecular Imaging and Biology. 2011; 13:1043–1049. [PubMed: 20835767]

Croce AC, Spano A, Balzarini P, Locatelli D, Barni S, Pippia P, et al. Proceedings of SPIE 2926, Optical Biopsies and Microscopic Techniques. 1996; 108:108–112.

DaCosta RS, Andersson H, Wilson BC. Molecular fluorescence excitation-emission matrices relevant to tissue spectroscopy. Photochemistry and Photobiology. 2003; 78:384–392. [PubMed: 14626667]

Darne CD, Lu Y, Tan IC, Zhu B, Rasmussen JC, Smith AM, et al. A compact frequency-domain photon migration system for integration into commercial hybrid small animal imaging scanners for fluorescence tomography. Physics in Medicine and Biology. 2012; 57:8135–8152. [PubMed: 23171509]

De Grand AM, Frangioni JV. An operational near-infrared fluorescence imaging system prototype for large animal surgery. Technology in Cancer Research & Treatment. 2003; 2:553–562. [PubMed: 14640766]

Demicheli R, Valagussa P, Bonadonna G. Does surgery modify growth kinetics of breast cancer micrometastases? British Journal of Cancer. 2001; 85:490–492. [PubMed: 11506484]

Evans CL, Potma EO, Puoris'haag M, Cote D, Lin CP, Xie XS. Chemical imaging of tissue in vivo with video-rate coherent anti-Stokes Raman scattering microscopy. Proceedings of the National Academy of Sciences of the United States of America. 2005; 102:16807–16812. [PubMed: 16263923]

Ferrante G, Presbitero P, Whitbourn R, Barlis P. Current applications of optical coherence tomography for coronary intervention. International Journal of Cardiology. 2013; 165:7–16. [PubMed: 22405134]

Ferroli P, Acerbi F, Albanese E, Tringali G, Broggi M, Franzini A, et al. Application of intraoperative indocyanine green angiography for CNS tumors: results on the first 100 cases. Acta Neurochirurgica. Supplement. 2011; 109:251–257. [PubMed: 20960352]

Flum DR, Koepsell T, Heagerty P, Sinanan M, Dellinger EP. Common bile duct injury during laparoscopic cholecystectomy and the use of intraoperative cholangiography: adverse outcome or preventable error? Archives of Surgery. 2001; 136:1287–1292. [PubMed: 11695975]

Folli S, Wagnieres G, Pelegrin A, Calmes JM, Braichotte D, Buchegger F, et al. Immunophotodiagnosis of colon carcinomas in patients injected with fluoresceinated chimeric antibodies against carcinoembryonic antigen. Proceedings of the National Academy of Sciences of the United States of America. 1992; 89:7973–7977. [PubMed: 1518823]

Fujiwara M, Mizukami T, Suzuki A, Fukamizu H. Sentinel lymph node detection in skin cancer patients using real-time fluorescence navigation with indocyanine green: preliminary experience. Journal of Plastic, Reconstructive & Aesthetic Surgery. 2009; 62:373–378.

Gioux S, Choi HS, Frangioni JV. Image-guided surgery using invisible near-infrared light: fundamentals of clinical translation. Molecular Imaging. 2010; 9:237–255. [PubMed: 20868625]

Giuliano AE, Kirgan DM, Guenther JM, Morton DL. Lymphatic mapping and sentinel lymphadenectomy for breast cancer. Annals of Surgery. 1994; 220:391–401. [PubMed: 8092905]

Gotoh K, Yamada T, Ishikawa O, Takahashi H, Eguchi H, Yano M, et al. A novel image-guided surgery of hepatocellular carcinoma by indocyanine green fluorescence imaging navigation. Journal of Surgical Oncology. 2009; 100:75–79. [PubMed: 19301311]

Gruev V, Perkins R, York T. CCD polarization imaging sensor with aluminum nanowire optical filters. Optics Express. 2010; 18:19087–19094. [PubMed: 20940803]

Handa T, Katare RG, Nishimori H, Wariishi S, Fukutomi T, Yamamoto M, et al. New device for intraoperative graft assessment: HyperEye charge-coupled device camera system. General Thoracic and Cardiovascular Surgery. 2010; 58:68–77. [PubMed: 20155342]

Hojo M, Arakawa Y, Funaki T, Yoshida K, Kikuchi T, Takagi Y, et al. Usefulness of Tumor Blood Flow Imaging by Intraoperative Indocyanine Green Videoangiography in Hemangioblastoma Surgery. World Neurosurgery. 2013 Epub ahead of print.

Huang D, Swanson E, Lin C, Schuman J, Stinson W, Chang W, et al. Optical coherence tomography. Science. 1991; 254:1178–1181. [PubMed: 1957169]

Hutteman M, Choi HS, Mieog JS, van der Vorst JR, Ashitate Y, Kuppen PJ, et al. Clinical translation of ex vivo sentinel lymph node mapping for colorectal cancer using invisible near-infrared fluorescence light. Annals of Surgical Oncology. 2011; 18:1006–1014. [PubMed: 21080086]

Hutteman M, van der Vorst JR, Gaarenstroom KN, Peters AA, Mieog JS, Schaafsma BE, et al. Optimization of near-infrared fluorescent sentinel lymph node mapping for vulvar cancer. American Journal of Obstetrics and Gynecology. 2012; 206:1–5. [PubMed: 22196682]

Hwang SW, Malek AM, Schapiro R, Wu JK. Intraoperative use of indocyanine green fluorescence videography for resection of a spinal cord hemangioblastoma. Neurosurgery. 2010; 67:300–303.

Ishizawa T, Bandai Y, Ijichi M, Kaneko J, Hasegawa K, Kokudo N. Fluorescent cholangiography illuminating the biliary tree during laparoscopic cholecystectomy. The British Journal of Surgery. 2010; 97:1369–1377. [PubMed: 20623766]

Ishizawa T, Fukushima N, Shibahara J, Masuda K, Tamura S, Aoki T, et al. Real-time identification of liver cancers by using indocyanine green fluorescent imaging. Cancer. 2009; 115:2491–2504. [PubMed: 19326450]

Ishizuka M, Kubota K, Kita J, Shimoda M, Kato M, Sawada T. Intraoperative observation using a fluorescence imaging instrument during hepatic resection for liver metastasis from colorectal cancer. Hepatogastroenterology. 2012; 59:90–92. [PubMed: 22260827]

Jacobs L. Positive margins: The challenge continues for breast surgeons. Annals of Surgical Oncology. 2008; 15:1271–1272. [PubMed: 18320287]

Jang I-K, Bouma BE, Kang D-H, Park S-J, Park S-W, Seung K-B, et al. Visualization of coronary atherosclerotic plaques in patients using optical coherence tomography: comparison with intravascular ultrasound. Journal of the American College of Cardiology. 2002; 39:604–609. [PubMed: 11849858]

Jayaprakash V, Sullivan M, Merzianu M, Rigual NR, Loree TR, Popat SR, et al. Autofluorescence-Guided Surveillance for Oral Cancer. Cancer Prevention Research. 2009; 2:966–974. [PubMed: 19892665]

Jocham D, Stepp H, Waidelich R. Photodynamic diagnosis in urology: state-of-the-art. European Urology. 2008; 53:1138–1148. [PubMed: 18096307]

Johansson, R.; Storm, A.; Stephansen, C.; Eikedal, S.; Willassen, T.; Skaug, S., et al. Solid-State Circuits Conference Digest of Technical Papers (ISSCC), 2011 IEEE International; 2011. p. 414-415.

Jolesz, FA. Intraoperative imaging and image-guided therapy. SpringerLink; 2014.

Joos KM, Shen J-H. Miniature real-time intraoperative forward-imaging optical coherence tomography probe. Biomedical Optics Express. 2013; 4:1342–1350. [PubMed: 24009997]

Kane RA. Intraoperative ultrasonography: history, current state of the art, and future directions. Journal of Ultrasound in Medicine. 2004; 23:1407–1420. [PubMed: 15498905]

Keaveny TV, Fitzgerald PA, McMullin JP. Selective parathyroid and pancreatic staining. The British Journal of Surgery. 1969; 56:595–597. [PubMed: 4183792]

Keaveny TV, Tawes R, Belzer FO. A new method for intra-operative identification of insulinomas. The British Journal of Surgery. 1971; 58:233–234. [PubMed: 4100889]

Keereweer S, Kerrebijn JD, van Driel PB, Xie B, Kaijzel EL, Snoeks TJ, et al. Optical image-guided surgery--where do we stand? Molecular Imaging and Biology. 2011; 13:199–207. [PubMed: 20617389]

Kim C, Erpelding TN, Maslov K, Jankovic L, Akers WJ, Song L, et al. Handheld array-based photoacoustic probe for guiding needle biopsy of sentinel lymph nodes. Journal of Biomedical Optics. 2010; 15:046010–046014. [PubMed: 20799812]

Koenig F, McGovern FJ, Althausen AF, Deutsch TF, Schomacker KT. Laser induced autofluorescence diagnosis of bladder cancer. The Journal of Urology. 1996; 156:1597–1601. [PubMed: 8863546]

Kraft JC, Ho RJ. Interactions of indocyanine green and lipid in enhancing near-infrared fluorescence properties: the basis for near-infrared imaging in vivo. Biochemistry. 2014; 53:1275–1283. [PubMed: 24512123]

Kubben PL, ter Meulen KJ, Schijns OE, ter Laak-Poort MP, van Overbeeke JJ, van Santbrink H. Intraoperative MRI-guided resection of glioblastoma multiforme: a systematic review. The Lancet Oncology. 2011; 12:1062–1070. [PubMed: 21868286]

Kunishige JH, Brodland DG, Zitelli JA. Surgical margins for melanoma in situ. Journal of the American Academy of Dermatology. 2012; 66:438–444. [PubMed: 22196979]

Kusano M, Tajima Y, Yamazaki K, Kato M, Watanabe M, Miwa M. Sentinel node mapping guided by indocyanine green fluorescence imaging: a new method for sentinel node navigation surgery in gastrointestinal cancer. Digestive Surgery. 2008; 25:103–108. [PubMed: 18379188]

LaRocca F, Nankivil D, Farsiu S, Izatt JA. Handheld simultaneous scanning laser ophthalmoscopy and optical coherence tomography system. Biomedical Optics Express. 2013; 4:2307–2321. [PubMed: 24298396]

Lee BT, Hutteman M, Gioux S, Stockdale A, Lin SJ, Ngo LH, et al. The FLARE intraoperative near-infrared fluorescence imaging system: a first-in-human clinical trial in perforator flap breast reconstruction. Plastic and Reconstructive Surgery. 2010; 126:1472–1481. [PubMed: 21042103]

Leong SP, Kim J, Ross M, Faries M, Scoggins CR, Metz WL, et al. A phase 2 study of (99m)Tc-tilmanocept in the detection of sentinel lymph nodes in melanoma and breast cancer. Annals of Surgical Oncology. 2011; 18:961–969. [PubMed: 21331809]

Lim YT, Kim S, Nakayama A, Stott NE, Bawendi MG, Frangioni JV. Selection of quantum dot wavelengths for biomedical assays and imaging. Molecular Imaging. 2003; 2:50–64. [PubMed: 12926237]

Liu Y, Akers WJ, Bauer AQ, Mondal S, Gullicksrud K, Sudlow GP, et al. Intraoperative detection of liver tumors aided by a fluorescence goggle system and multimodal imaging. Analyst. 2013a; 138:2254–2257. [PubMed: 23467534]

Liu Y, Bauer AQ, Akers WJ, Sudlow G, Liang K, Shen D, et al. Hands-free, wireless goggles for near-infrared fluorescence and real-time image-guided surgery. Surgery. 2011; 149:689–698. [PubMed: 21496565]

Liu Y, Brand RE, Turzhitsky V, Kim YL, Roy HK, Hasabou N, et al. Optical markers in duodenal mucosa predict the presence of pancreatic cancer. Clinical Cancer Research. 2007; 13:4392–4399. [PubMed: 17671121]

Liu Y, Njuguna R, Matthews T, Akers WJ, Sudlow GP, Mondal S, et al. Near-infrared fluorescence goggle system with complementary metal-oxide-semiconductor imaging sensor and see-through display. Journal of Biomedical Optics. 2013b; 18:101303. [PubMed: 23728180]

Liu Y, York T, Akers W, Sudlow G, Gruev V, Achilefu S. Complementary fluorescence-polarization microscopy using division-of-focal-plane polarization imaging sensor. Journal of Biomedical Optics. 2012; 17:116001. [PubMed: 23117796]

Liu Y, Zhao YM, Akers W, Tang ZY, Fan J, Sun HC, et al. First in-human intraoperative imaging of HCC using the fluorescence goggle system and transarterial delivery of near-infrared fluorescent imaging agent: a pilot study. Translational Research. 2013c; 162:324–331. [PubMed: 23747795]

Lu CD, Kraus MF, Potsaid B, Liu JJ, Choi W, Jayaraman V, et al. Handheld ultrahigh speed swept source optical coherence tomography instrument using a MEMS scanning mirror. Biomedical Optics Express. 2014; 5:293–311. [PubMed: 24466495]

Lucia Pelosini HBS, John B Schofield, Meeckings Adam, Dhital Anish, Khandwala Mona. In vivo optical coherence tomography (OCT) in periocular basal cell carcinoma: correlations between in

vivo OCT images and postoperative histology. British Journal of Ophthalmology. 2013; 97:890–894. [PubMed: 23677987]

Marshall MV, Rasmussen JC, Tan IC, Aldrich MB, Adams KE, Wang X, et al. Near-Infrared Fluorescence Imaging in Humans with Indocyanine Green: A Review and Update. Open Surgical Oncology Journal. 2010; 2:12–25.

Matsui A, Lee BT, Winer JH, Vooght CS, Laurence RG, Frangioni JV. Real-time intraoperative near-infrared fluorescence angiography for perforator identification and flap design. Plastic and Reconstructive Surgery. 2009; 123:125–127.

Matsui A, Tanaka E, Choi HS, Winer JH, Kianzad V, Gioux S, et al. Real-time intra-operative near-infrared fluorescence identification of the extrahepatic bile ducts using clinically available contrast agents. Surgery. 2010; 148:87–95. [PubMed: 20117813]

Mieog JS, Troyan SL, Hutteman M, Donohoe KJ, van der Vorst JR, Stockdale A, et al. Toward optimization of imaging system and lymphatic tracer for near-infrared fluorescent sentinel lymph node mapping in breast cancer. Annals of Surgical Oncology. 2011; 18:2483–2491. [PubMed: 21360250]

Mieog JS, Vahrmeijer AL, Hutteman M, van der Vorst JR, Drijfhout van Hooff M, Dijkstra J, et al. Novel intraoperative near-infrared fluorescence camera system for optical image-guided cancer surgery. Molecular Imaging. 2010; 9:223–231. [PubMed: 20643025]

Miranda-Sousa AJ, Davila HH, Lockhart JL, Ordorica RC, Carrion RE. Sexual function after surgery for prostate or bladder cancer. Cancer Control. 2006; 13:179–187. [PubMed: 16885913]

Mislow JM, Golby AJ, Black PM. Origins of intraoperative MRI. Neurosurgery Clinics of North America. 2009; 20:137–146. [PubMed: 19555875]

Mitsunaga M, Kosaka N, Choyke PL, Young MR, Dextras CR, Saud SM, et al. Fluorescence endoscopic detection of murine colitis-associated colon cancer by topically applied enzymatically rapid-activatable probe. Gut. 2013; 62:1179–1186. [PubMed: 22698650]

Miyashiro I, Miyoshi N, Hiratsuka M, Kishi K, Yamada T, Ohue M, et al. Detection of sentinel node in gastric cancer surgery by indocyanine green fluorescence imaging: comparison with infrared imaging. Annals of Surgical Oncology. 2008; 15:1640–1643. [PubMed: 18379850]

Moiyadi A, Syed P, Srivastava S. Fluorescence-guided surgery of malignant gliomas based on 5-aminolevulinic acid: paradigm shifts but not a panacea. Nature Reviews. Cancer. 2014; 14:146.

Moller MG, Pappas-Politis E, Zager JS, Santiago LA, Yu D, Prakash A, et al. Surgical management of melanoma-in-situ using a staged marginal and central excision technique. Annals of Surgical Oncology. 2009; 16:1526–1536. [PubMed: 19050971]

Mondal SB, Gao S, Zhu N, Liu Y, Sudlow GP, Akers WJ, et al. Proc. SPIE 8936, Design and Quality for Biomedical Technologies VII. 2014:89360–89365.

Moore GE. Fluorescein as an Agent in the Differentiation of Normal and Malignant Tissues. Science. 1947; 106:130–131. [PubMed: 17750790]

Moore GE, Peyton WT, et al. The clinical use of fluorescein in neurosurgery; the localization of brain tumors. Journal of Neurosurgery. 1948; 5:392–398. [PubMed: 18872412]

Morton DL, Bostick PJ. Will the true sentinel node please stand? Annals of Surgical Oncology. 1999; 6:12–14. [PubMed: 10030408]

Nguyen FT, Zysk AM, Chaney EJ, Kotynek JG, Oliphant UJ, Bellafiore FJ, Rowland KM, Johnson PA, Boppart SA. Intraoperative Evaluation of Breast Tumor Margins with Optical Coherence Tomography. Cancer Research. 2009; 69:8790–8796. [PubMed: 19910294]

Nguyen QT, Tsien RY. Fluorescence-guided surgery with live molecular navigation -- a new cutting edge. Nature Reviews. Cancer. 2013; 13:653–662.

Nimura H, Narimiya N, Mitsumori N, Yamazaki Y, Yanaga K, Urashima M. Infrared ray electronic endoscopy combined with indocyanine green injection for detection of sentinel nodes of patients with gastric cancer. The British Journal of Surgery. 2004; 91:575–579. [PubMed: 15122608]

Palanker DV, Blumenkranz MS, Andersen D, Wiltberger M, Marcellino G, Gooding P, et al. Femtosecond Laser-Assisted Cataract Surgery with Integrated Optical Coherence Tomography. Science Translational Medicine. 2010; 2:58–85.

Paul Hahn JM, Rachelle O'Connell, Ramiro S. Maldonado Joseph A. Izatt, Cynthia A. Toth. The Use of Optical Coherence Tomography in Intraoperative Ophthalmic Imaging. Ophthalmic Surgery, Lasers and Imaging Retina. 2011; 42:85–94.

Peloso A, Franchi E, Canepa MC, Barbieri L, Briani L, Ferrario J, et al. Combined use of intraoperative ultrasound and indocyanine green fluorescence imaging to detect liver metastases from colorectal cancer. International Hepato-Pancreato-Biliary Association (Oxford). 2013; 15:928–934.

Poh CF, MacAulay CE, Zhang L, Rosin MP. Tracing the "at-risk" oral mucosa field with autofluorescence: steps toward clinical impact. Cancer Prevention Research. 2009; 2:401–404. [PubMed: 19401533]

Poh CF, Zhang LW, Anderson DW, Durham JS, Williams RM, Priddy RW, et al. Fluorescence visualization detection of field alterations in tumor margins of oral cancer patients. Clinical Cancer Research. 2006; 12:6716–6722. [PubMed: 17121891]

Ramanujam N. Fluorescence spectroscopy of neoplastic and non-neoplastic tissues. Neoplasia. 2000; 2:89–117. [PubMed: 10933071]

Ramanujam N, Mitchell MF, Mahadevan A, Warren S, Thomsen S, Silva E, et al. In vivo diagnosis of cervical intraepithelial neoplasia using 337-nm-excited laser-induced fluorescence. Proceedings of the National Academy of Sciences of the United States of America. 1994; 91:10193–10197. [PubMed: 7937860]

Ramiro S. Maldonado JAI, Neeru Sarin David K. Wallace, Sharon Freedman C. Michael Cotten, Cynthia A. Toth. Optimizing Hand-held Spectral Domain Optical Coherence Tomography Imaging for Neonates, Infants, and Children. Investigative Ophthalmology & Visual Science. 2010; 51:2678–2685. [PubMed: 20071674]

Rassmussen-Taxdal DS, Ward GE, Figge FHJ. Fluorescence of human lymphatic and cancer tissues following high doses of intravenous hematoporphyrin. Cancer. 1955; 8:78–81. [PubMed: 13231035]

Retsky M, Bonadonna G, Demicheli R, Folkman J, Hrushesky W, Valagussa P. Hypothesis: Induced angiogenesis after surgery in premenopausal node-positive breast cancer patients is a major underlying reason why adjuvant chemotherapy works particularly well for those patients. Breast Cancer Research. 2004; 6:372–374.

Ries, LAG.; Melbert, D.; Krapcho, M.; Stinchcomb, DG.; Howlader, N.; Horner, MJ., et al. SEER cancer statistics review, 1975–2005. U.S. National Institutes of Health, National Cancer Institute; Bethesda, MD: 2008.

Sahani DV, Kalva SP, Tanabe KK, Hayat SM, O'Neill MJ, Halpern EF, et al. Intraoperative US in patients undergoing surgery for liver neoplasms: comparison with MR imaging. Radiology. 2004; 232:810–814. [PubMed: 15273336]

Satou S, Ishizawa T, Masuda K, Kaneko J, Aoki T, Sakamoto Y, et al. Indocyanine green fluorescent imaging for detecting extrahepatic metastasis of hepatocellular carcinoma. Journal of Gastroenterology. 2013; 48:1136–1143. [PubMed: 23179608]

Schaafsma BE, Mieog JS, Hutteman M, van der Vorst JR, Kuppen PJ, Lowik CW, et al. The clinical use of indocyanine green as a near-infrared fluorescent contrast agent for image-guided oncologic surgery. J Surg Oncol. 2011a; 104:323–332. [PubMed: 21495033]

Schaafsma BE, Mieog JS, Hutteman M, van der Vorst JR, Kuppen PJ, Lowik CW, et al. The clinical use of indocyanine green as a near-infrared fluorescent contrast agent for image-guided oncologic surgery. Journal of Surgical Oncology. 2011b; 104:323–332. [PubMed: 21495033]

Sekijima M, Tojimbara T, Sato S, Nakamura M, Kawase T, Kai K, et al. An intraoperative fluorescent imaging system in organ transplantation. Transplantation Proceedings. 2004; 36:2188–2190. [PubMed: 15518796]

Selzman AA, Spirnak JP. Iatrogenic ureteral injuries: a 20-year experience in treating 165 injuries. The Journal of Urology. 1996; 155:878–881. [PubMed: 8583597]

Sevick-Muraca EM, Rasmussen JC. Molecular imaging with optics: primer and case for near-infrared fluorescence techniques in personalized medicine. Journal of Biomed Optics. 2008; 13:041303–041316.

Sexton K, Davis SC, McClatchy D, Valdes PA, Kanick SC, Paulsen KD, et al. Pulsed-light imaging for fluorescence guided surgery under normal room lighting. Optics Letters. 2013; 38:3249–3252. [PubMed: 23988926]

Shinoda J, Yano H, Yoshimura S, Okumura A, Kaku Y, Iwama T, et al. Fluorescence-guided resection of glioblastoma multiforme by using high-dose fluorescein sodium. Technical note. Journal of Neurosurgery. 2003; 99:597–603. [PubMed: 12959452]

Siegel R, Ma J, Zou Z, Jemal A. Cancer statistics, 2014. CA: A Cancer Journal for Clinicians. 2014; 64:9–29. [PubMed: 24399786]

Skripenova S, Layfield LJ. Initial margin status for invasive ductal carcinoma of the breast and subsequent identification of carcinoma in reexcision specimens. Archives of Pathology & Laboratory Medicine. 2010; 134:109–114. [PubMed: 20073613]

Smith AM, Mancini MC, Nie S. Bioimaging: second window for in vivo imaging. Nature Nanotechnology. 2009; 4:710–711.

Spinoglio G, Priora F, Bianchi PP, Lucido FS, Licciardello A, Maglione V, et al. Real-time near-infrared (NIR) fluorescent cholangiography in single-site robotic cholecystectomy (SSRC): a single-institutional prospective study. Surgical Endoscopy. 2013; 27:2156–2162. [PubMed: 23271272]

Stummer W, Pichlmeier U, Meinel T, Wiestler OD, Zanella F, Reulen HJ. Fluorescence-guided surgery with 5-aminolevulinic acid for resection of malignant glioma: a randomised controlled multicentre phase III trial. The Lancet Oncology. 2006; 7:392–401. [PubMed: 16648043]

Tagaya N, Yamazaki R, Nakagawa A, Abe A, Hamada K, Kubota K, et al. Intraoperative identification of sentinel lymph nodes by near-infrared fluorescence imaging in patients with breast cancer. American Journal of Surgery. 2008; 195:850–853. [PubMed: 18353274]

Takahashi M, Ishikawa T, Higashidani K, Katoh H. SPY: an innovative intra-operative imaging system to evaluate graft patency during off-pump coronary artery bypass grafting. Interactive Cardiovascular and Thoracic Surgery. 2004; 3:479–483. [PubMed: 17670291]

Tanaka E, Chen FY, Flaumenhaft R, Graham GJ, Laurence RG, Frangioni JV. Real-time assessment of cardiac perfusion, coronary angiography, and acute intravascular thrombi using dual-channel near-infrared fluorescence imaging. The Journal of Thoracic and Cardiovascular Surgery. 2009; 138:133–140. [PubMed: 19577070]

Tanis PJ, Nieweg OE, Valdes Olmos RA, Th Rutgers EJ, Kroon BB. History of sentinel node and validation of the technique. Breast Cancer Research. 2001; 3:109–112. [PubMed: 11250756]

Tao YK, Ehlers JP, Toth CA, Izatt JA. Intraoperative spectral domain optical coherence tomography for vitreoretinal surgery. Optics Letters. 2010; 35:3315–3317. [PubMed: 20967051]

Themelis G, Yoo JS, Soh KS, Schulz R, Ntziachristos V. Real-time intraoperative fluorescence imaging system using light-absorption correction. Journal of Biomedical Optics. 2009; 14:064012–064019. [PubMed: 20059250]

Ting R, Aguilera TA, Crisp JL, Hall DJ, Eckelman WC, Vera DR, et al. Fast 18F labeling of a near-infrared fluorophore enables positron emission tomography and optical imaging of sentinel lymph nodes. Bioconjugate Chemistry. 2010; 21:1811–1819. [PubMed: 20873712]

Troyan SL, Kianzad V, Gibbs-Strauss SL, Gioux S, Matsui A, Oketokoun R, et al. The FLARE intraoperative near-infrared fluorescence imaging system: a first-in-human clinical trial in breast cancer sentinel lymph node mapping. Annals of Surgical Oncology. 2009; 16:2943–2952. [PubMed: 19582506]

Tsujino Y, Mizumoto K, Matsuzaka Y, Niihara H, Morita E. Fluorescence navigation with indocyanine green for detecting sentinel nodes in extramammary Paget's disease and squamous cell carcinoma. The Journal of Dermatology. 2009; 36:90–94. [PubMed: 19284452]

Uchiyama K, Ueno M, Ozawa S, Kiriyama S, Shigekawa Y, Yamaue H. Combined use of contrast-enhanced intraoperative ultrasonography and a fluorescence navigation system for identifying hepatic metastases. World Journal of Surgery. 2010; 34:2953–2959. [PubMed: 20734045]

Ukimura O, Okihara K, Kamoi K, Naya Y, Ochiai A, Miki T. Intraoperative ultrasonography in an era of minimally invasive urology. International Journal of Urology. 2008; 15:673–680. [PubMed: 18564203]

Vahrmeijer AL, Hutteman M, van der Vorst JR, van de Velde CJH, Frangioni JV. Image-guided cancer surgery using near-infrared fluorescence. Nature Reviews. Clinical Oncology. 2013; 10:507–518.

Valdes PA, Leblond F, Kim A, Harris BT, Wilson BC, Fan X, et al. Quantitative fluorescence in intracranial tumor: implications for ALA-induced PpIX as an intraoperative biomarker. Journal of Neurosurgery. 2011; 115:11–17. [PubMed: 21438658]

van Dam GM, Themelis G, Crane LM, Harlaar NJ, Pleijhuis RG, Kelder W, et al. Intraoperative tumor-specific fluorescence imaging in ovarian cancer by folate receptor-alpha targeting: first in-human results. Nature Medicine. 2011; 17:1315–1319.

van den Berg NS, Brouwer OR, Klop WM, Karakullukcu B, Zuur CL, Tan IB, et al. Concomitant radio- and fluorescence-guided sentinel lymph node biopsy in squamous cell carcinoma of the oral cavity using ICG-(99m)Tc-nanocolloid. European Journal of Nuclear Medicine and Molecular Imaging. 2012; 39:1128–1136. [PubMed: 22526966]

van der Poel HG, Buckle T, Brouwer OR, Valdes Olmos RA, van Leeuwen FW. Intraoperative laparoscopic fluorescence guidance to the sentinel lymph node in prostate cancer patients: clinical proof of concept of an integrated functional imaging approach using a multimodal tracer. European Urology. 2011; 60:826–833. [PubMed: 21458154]

van der Vorst JR, Hutteman M, Gaarenstroom KN, Peters AA, Mieog JS, Schaafsma BE, et al. Optimization of near-infrared fluorescent sentinel lymph node mapping in cervical cancer patients. International Journal of Gynecological Cancer. 2011; 21:1472–1478. [PubMed: 22027751]

van der Vorst JR, Schaafsma BE, Verbeek FP, Hutteman M, Mieog JS, Lowik CW, et al. Randomized comparison of near-infrared fluorescence imaging using indocyanine green and 99(m) technetium with or without patent blue for the sentinel lymph node procedure in breast cancer patients. Annals of Surgical Oncology. 2012a; 19:4104–4111. [PubMed: 22752379]

van der Vorst JR, Vahrmeijer AL, Hutteman M, Bosse T, Smit VT, van de Velde CJ, et al. Near-infrared fluorescence imaging of a solitary fibrous tumor of the pancreas using methylene blue. World journal of Gastrointestinal Surgery. 2012b; 4:180–184. [PubMed: 22905287]

van Vledder MG, Torbenson MS, Pawlik TM, Boctor EM, Hamper UM, Olino K, et al. The effect of steatosis on echogenicity of colorectal liver metastases on intraoperative ultrasonography. Archives of Surgery. 2010; 145:661–667. [PubMed: 20644129]

Varghese P, Abdel-Rahman AT, Akberali S, Mostafa A, Gattuso JM, Carpenter R. Methylene blue dye--a safe and effective alternative for sentinel lymph node localization. The Breast Journal. 2008; 14:61–67. [PubMed: 18186867]

Vera DR, Wallace AM, Hoh CK, Mattrey RF. A synthetic macromolecule for sentinel node detection: (99m)Tc-DTPA-mannosyl-dextran. Journal of Nuclear Medicine. 2001; 42:951–959. [PubMed: 11390562]

Verbeek FP, van der Vorst JR, Schaafsma BE, Hutteman M, Bonsing BA, van Leeuwen FW, et al. Image-guided hepatopancreatobiliary surgery using near-infrared fluorescent light. Journal of Hepato-biliary-pancreatic Sciences. 2012; 19:626–637. [PubMed: 22790312]

Vicini FA, Kestin LL, Goldstein NS, Chen PY, Pettinga J, Frazier RC, et al. Impact of young age on outcome in patients with ductal carcinoma-in-situ treated with breast-conserving therapy. Journal of Clinical Oncology. 2000; 18:296–306. [PubMed: 10637243]

Wallner C, Lange MM, Bonsing BA, Maas CP, Wallace CN, Dabhoiwala NF, et al. Causes of fecal and urinary incontinence after total mesorectal excision for rectal cancer based on cadaveric surgery: a study from the Cooperative Clinical Investigators of the Dutch total mesorectal excision trial. Journal of Clinical Oncology. 2008; 26:4466–4472. [PubMed: 18802159]

Weissleder R, Pittet MJ. Imaging in the era of molecular oncology. Nature. 2008; 452:580–589. [PubMed: 18385732]

Wilke LG, Brown JQ, Bydlon TM, Kennedy SA, Richards LM, Junker MK, et al. Rapid noninvasive optical imaging of tissue composition in breast tumor margins. American Journal of Surgery. 2009; 198:566–574. [PubMed: 19800470]

Winer JH, Choi HS, Gibbs-Strauss SL, Ashitate Y, Colson YL, Frangioni JV. Intraoperative localization of insulinoma and normal pancreas using invisible near-infrared fluorescent light. Annals of Surgical Oncology. 2010a; 17:1094–1100. [PubMed: 20033320]

Winer JH, Choi HS, Gibbs-Strauss SL, Ashitate Y, Colson YL, Frangioni JV. Intraoperative localization of insulinoma and normal pancreas using invisible near-infrared fluorescent light. Ann Surg Oncol. 2010b; 17:1094–1100. [PubMed: 20033320]

Woonggyu Jung JK, Mansik Jeon Eric J. Chaney, Charles N. Stewart, Stephen A. Boppart. Handheld Optical Coherence Tomography Scanner for Primary Care Diagnostics. IEEE Trans Biomed Engineering. 2012; 58:9.

Yabroff KR, Lund J, Kepka D, Mariotto A. Economic burden of cancer in the United States: estimates, projections, and future research. Cancer Epidemiology, Biomarkers & Prevention. 2011; 20:2006–2014.

Yokoyama N, Otani T, Hashidate H, Maeda C, Katada T, Sudo N, et al. Real-time detection of hepatic micrometastases from pancreatic cancer by intraoperative fluorescence imaging: preliminary results of a prospective study. Cancer. 2012; 118:2813–2819. [PubMed: 21990070]

Zhang X, Shoushun C, Culurciello E. Sensors, 2011 IEEE. 2011:1933–1936.

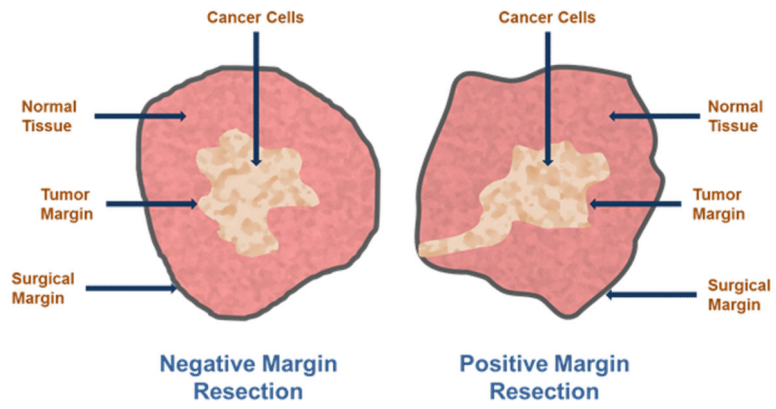**Fig 1.**
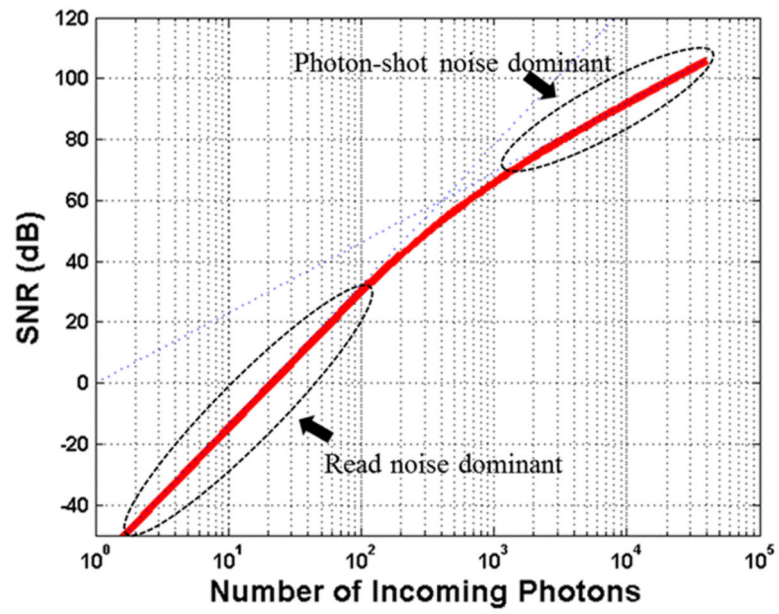Cartoon of surgical margins of resection in breast cancer.

Figure 2.
Model of signal-to-noise ratio of an imaging sensor with read-out noise of 10e⁻ and maximum well depth capacity of 100ke⁻
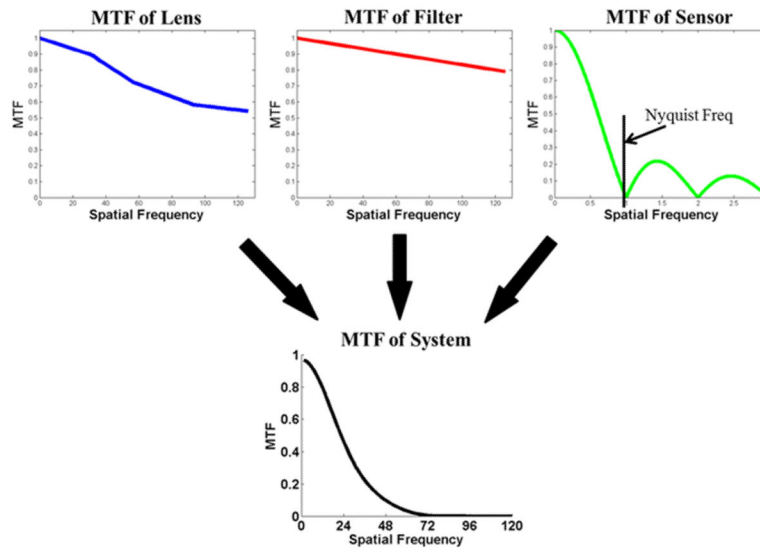
Figure 3.
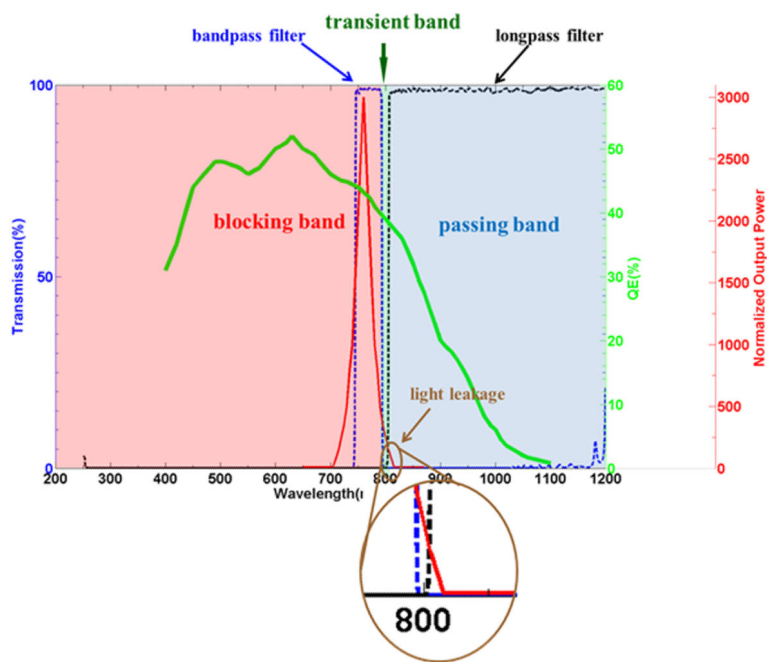MTF of fluorescent imaging system and components

Figure 4.
Fluorescent system setup example. Dotted lines show the transmission of the corresponding filters. The blue dotted line is the bandpass filter used to trim the excitation light, the black dotted line is the longpass filter to keep the emitting light. Green solid line shows QE of the imager, and red solid line is the spectral response of the LED output light. The brown circle marks the light leakage from the excitation light.
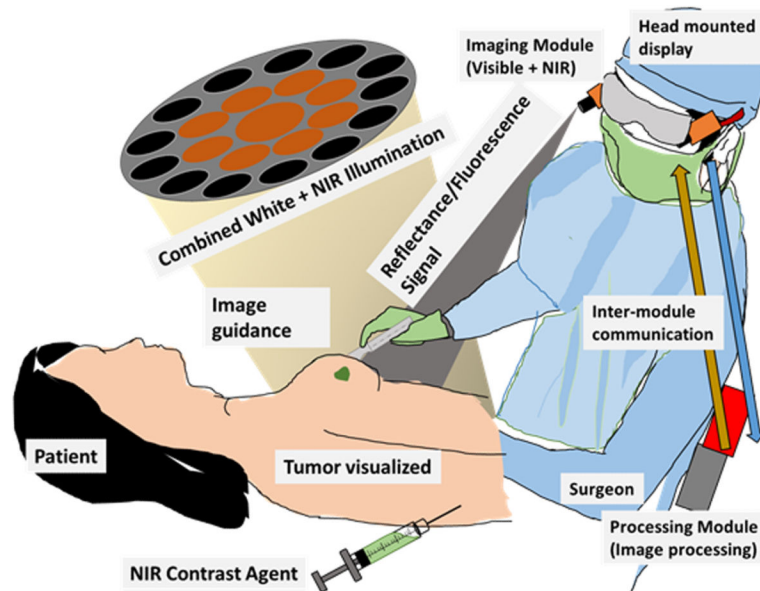
Figure 5.
Goggle system overview. After injection of an imaging agent, our system excites the contrast agent. The NIR fluorescence and color reflectance images are captured and processed to generate a superimposed image where fluorescence is highlighted in a false color on the normal view. This superimposed image is seen in the head mounted display in real time by the surgeon, who can clearly visualize the tumor boundary during cancer surgery.

Table 1

Desirable characteristics for real-time image guidance surgery

Characteristic	Description
Intraoperative	Hardware conducive to be used in the operating room, during surgery
Real-time	24p frames per second image acquisition and display to surgeon without latency
High specificity	Contrast agent that very specifically accumulates in the tumor being imaged. Low false negatives
High sensitivity	High detection sensitivity of imaging system Detection of low fluorescence signal and small tumors
High resolution	Detection of small tumors and interrogation of the tumor boundary
Wearable	Ergonomic, hands-free unrestrictive movement
Non-interfering	Information display in a form that does not distract surgeon from the surgical bed
User friendly	Requires minimal training and no specialized operators

Table 2

Representative fluorescence image-guided systems

System	Real-time	NIR-color overlay	Display	Status	References
Mounted					
SPY		No	Remote Monitor	Commercially available. FDA approved	(Sekijima, M., Tojimbara, T., Sato, S., Nakamura, M., Kawase, T., Kai, K. et al., 2004; Takahashi, M., Ishikawa, T., Higashidani, K. and Katoh, H., 2004)
FLARE	Yes	Yes	Remote Monitor	Clinical Studies	(Troyan, S. L., Kianzad, V., Gibbs-Strauss, S. L., Gioux, S., Matsui, A., Oketokoun, R. et al., 2009)
SurgOptix	Yes	Yes	Remote Monitor	Clinical Studies	(Crane, L. M., Themelis, G., Pleijhuis, R. G., Harlaar, N. J., Sarantopoulos, A., Arts, H. J. et al., 2011; Themelis, G., Yoo, J. S., Soh, K. S., Schulz, R. and Ntziachristos, V., 2009; van Dam, G. M., Themelis, G., Crane, L. M., Harlaar, N. J., Pleijhuis, R. G., Kelder, W. et al., 2011)
ArteMIS	Yes	No	Remote Display	Commercially available	(Keereweer, S., Kerrebijn, J. D., van Driel, P. B., Xie, B., Kaijzel, E. L., Snoeks, T. J. et al., 2011)
HyperEye	Yes		Remote Display	Experimental	(Handa, T., Katare, R. G., Nishimori, H., Wariishi, S., Fukutomi, T., Yamamoto, M. et al., 2010)
FDPM	No		Remote Display	Experimental	(Darne, C. D., Lu, Y., Tan, I. C, Zhu, B., Rasmussen, J. C, Smith, A. M. et al., 2012; Marshall, M. V., Rasmussen, J. C, Tan, I. C, Aldrich, M. B., Adams, K. E., Wang, X. et al., 2010)
Handheld					
Fluobeam		Yes	Remote display	Commercially available	(Mieog, J. S., Vahrmeijer, A. L., Hutteman, M., van der Vorst, J. R., Drijfhout van Hooff, M., Dijkstra, J. et al., 2010)
PDE		No	Remote display	Commercially available. FDA approved	(Tagaya, N., Yamazaki, R., Nakagawa, A., Abe, A., Hamada, K., Kubota, K. et al., 2008)
Wearable					
Goggle System		Yes	Head mounted display	Clinical studies.	(Liu, Y., Bauer, A. Q., Akers, W. J., Sudlow, G., Liang, K., Shen, D. et al., 2011; Mondal, S. B., Gao, S., Zhu, N., Liu, Y., Sudlow, G. P., Akers, W.J. et al., 2014)

Table 3

Representative fluorescence contrast agents used for real-time image-guided surgery.

Agent	λ_{em} [a]	Tumor targeting	Applications	References
ICG	820 nm	EPR effect	SLNM in breast, skin, cervical cancer Tumor imaging in HCC Reconstructive surgery	(Hutteman, M., Choi, H. S., Mieog, J. S., van der Vorst, J. R., Ashitate, Y., Kuppen, P. J. et al., 2011; Hutteman, M., van der Vorst, J. R., Gaarenstroom, K. N., Peters, A. A., Mieog, J. S., Schaafsma, B. E. et al., 2012; Lee, B. T., Hutteman, M., Gioux, S., Stockdale, A., Lin, S. J., Ngo, L. H. et al., 2010; Troyan, S. L., Kianzad, V., Gibbs-Strauss, S. L., Gioux, S., Matsui, A., Oketokoun, R., et al., 2009; Verbeek, F. P., van der Vorst, J. R., Schaafsma, B. E., Hutteman, M., Bonsing, B. A., van Leeuwen, F. W. et al., 2012)
Fluorescein	520 nm	EPR effect	Image guided resection of glioblastoma	(Shinoda, J., Yano, H., Yoshimura, S., Okumura, A., Kaku, Y., Iwama, T. et al., 2003)
Methylene Blue	680 nm	EPR effect	SLNM Insulinoma	(Varghese, P., Abdel-Rahman, A. T., Akberali, S., Mostafa, A., Gattuso, J. M. and Carpenter, R, 2008; Winer, J. H., Choi, H. S., Gibbs-Strauss, S. L., Ashitate, Y., Colson, Y. L. and Frangioni, J. V., 2010)
5-ALA	635 nm	Porphyrin expression	Glioma resection Glioma grade biomarker	(Stummer, W., Pichlmeier, U., Meinel, T., Wiestler, O. D., Zanella, F. and Reulen, H. J., 2006; Valdes, P. A., Leblond, F., Kim, A., Harris, B. T., Wilson, B. C, Fan, X. et al., 2011)
LS 301	780 nm 820 nm	Redox potential	Tumor visualizatio Tumor margin assessment	(Liu, Y., Akers, W. J., Bauer, A. Q., Mondal, S., Gullicksrud, K., Sudlow, G. P. et al., 2013; Liu, Y., Bauer, A. Q., Akers, W. J., Sudlow, G., Liang, K., Shen, D., et al., 2011; Liu, Y., Njuguna, R, Matthews, T., Akers, W. J., Sudlow, G. P., Mondal, S. et al., 2013; Liu, Y., Zhao, Y. M., Akers, W., Tang, Z. Y., Fan, J., Sun, H. C. et al., 2013; Mondal, S. B., Gao, S., Zhu, N., Liu, Y., Sudlow, G. P., Akers, W. J., et al., 2014)

EPR, enhanced permeability and retention.

[a]Peak fluorescence emission wavelength